



Integrating expected loss and collapse risk in performance-based seismic design of structures

Davit Shahnazaryan¹ · Gerard J. O'Reilly¹

Received: 14 May 2020 / Accepted: 7 November 2020
© Springer Nature B.V. 2021

Abstract

With the introduction of performance-based earthquake engineering (PBEE), engineers have strived to relate building performance to different seismic hazard levels. Expected annual loss (EAL) and collapse safety described by mean annual frequency of collapse (MAFC) have become employed more frequently, but tend to be limited to seismic assessment rather than design. This article outlines an integrated performance-based seismic design (IPBSD) method that uses EAL and MAFC as design parameters. With these, as opposed to conventional intensity-based strength and/or drift requirements, IPBSD limits expected monetary losses and maintains a sufficient and quantifiable level of collapse safety in buildings. Through simple procedures, it directly identifies feasible structural solutions without the need for detailed calculations and numerical analysis. This article outlines its implementation alongside other contemporary risk-targeted and code-based approaches. Several case study reinforced concrete frame structures are evaluated using these approaches and the results appraised via verification analysis. The agreement and consistency of the design solutions and the intended targets are evaluated to demonstrate the suitability of each method. The proposed framework is viewed as a stepping stone for seismic design with advanced performance objectives in line with modern PBEE requirements.

Keywords PBEE · Expected annual loss · Mean annual frequency of collapse · Risk-targeted design · Reinforced concrete

1 Introduction

Over the years, the earthquake engineering community has worked towards preventing damage of structural and non-structural elements in frequent low-intensity earthquakes and preventing collapse in rare high-intensity earthquakes. After the economic impact of the 1994 Northridge earthquake in the US due to extensive damage and overall disruption, an immediate shift was necessary for building performance definition. Traditional objectives of seismic codes or assessment frameworks, focusing on life safety and collapse prevention of buildings,

✉ Gerard J. O'Reilly
gerard.oreilly@iusspavia.it

¹ Scuola Universitaria Superiore IUSS di Pavia, Piazza della Vittoria 15, Pavia 27100, Italy

were not sufficient for complete satisfactory building performance. The change happened with the introduction of performance-based earthquake engineering (PBEE) during the latter half of the 1990s with the Vision 2000 framework (SEAOC 1995). It related desired building performance to various seismic hazard levels via the definition of limit states or performance levels. These were termed fully operational, operational, life-safe, and near-collapse, corresponding to hazard levels of frequent, occasional, rare, and very rare events, respectively. In the early 2000s, FEMA-356 (Emergency and Agency 2000) emerged and established element deformation and force-based acceptability criteria for different performance levels of structural and non-structural elements.

Following the initial interpretations of PBEE, a more robust and powerful probabilistic framework was developed and set the basis for what is known as the Pacific Earthquake Engineering Research (PEER) Centre PBEE methodology (Cornell and Krawinkler 2000). It centres around the idea of probabilistically quantifying the mean annual frequency of exceedance (MAFE), or failure, of a limit state, λ_f , by integrating the probability of failure for a chosen intensity measure (IM), $P[f|IM=im]$, with the site hazard curve, $H(im)$, as follows (Cornell et al. 2002):

$$\lambda_f = \int_0^{+\infty} P[f|IM=im] dH(im) \quad (1)$$

This modernised approach quantifies the building performance in an overall risk sense and is flexible in its definition of failure, allowing consistent consideration across all pertinent limit states (e.g. onset of structural/non-structural damage and collapse). Therefore, the overall performance of the building can be quantified via more meaningful metrics to building owners or stakeholders (e.g. casualties, economic losses, anticipated downtime). Due to the probabilistic nature of the framework and its computationally expensive implementation in certain situations, it has been largely popular within academic research or specialised reports (FEMA 2012; CNR 2014) rather than widespread code implementation for practitioners to use. Furthermore, given the nature of the framework, it has been predominantly developed for the assessment of existing buildings as opposed to the design of new ones.

With the evolution of PBEE concerning new design, this article builds on a framework recently proposed by O'Reilly and Calvi (2019). It utilises collapse risk alongside economic loss control in a simplified manner as the main design inputs and performance objectives remain consistent with the goals of PBEE (Vamvatsikos et al. 2016). This article first reviews risk-targeted design methods proposed in the literature along with current code-based approaches. The proposed framework is introduced and described in a step-by-step manner for the case of reinforced concrete (RC) frame structures. Application of these methods is investigated via several case study frame buildings to assess their ability in satisfying the required performance objectives in an efficient manner suitable for future building codes. This article focuses on the satisfaction of collapse risk requirements facet and these methods' ability to limit economic losses will be focused on in future work.

2 Seismic design of structures

2.1 Existing design code approaches

Current seismic design codes primarily focus on ensuring the life safety of building occupants by avoiding structural collapse. Additionally, performance at frequent levels of ground shaking is to be checked and verified. These are termed the *no-collapse requirement* and *damage limitation requirement* in the current version of Eurocode 8 (EC8) (CEN 2004b) and are implemented at ground shaking return periods of 475 and 95 years, respectively, with possible modifications to account for building importance class. New Zealand's NZS1170 (NZS 2004) defines two limits states, termed as *serviceability* and *ultimate* with design return periods of 25 and 500 years, respectively, with the possibility of modification for different importance classes similar to EC8. A slightly modified approach is outlined in the recently revised design code in the US, ASCE 7-16 (2016), where the building is designed using a fraction of the maximum considered event (MCE) as input, which is determined from a series of risk-targeted hazard maps developed for a target collapse risk of 1% in 50 years.

The design method employed in seismic design codes follows what may be referred to as force-based design (FBD). It calculates a design base shear force from a reduced elastic spectrum using either the equivalent lateral force (ELF) method or response spectrum method of analysis (RSMA). Despite seismic codes having the option to use non-linear numerical models for static pushover (SPO) analysis or non-linear response history analysis (NLRHA) with a set of suitable ground motion records, these approaches may be deemed too computationally expensive at times and not always implemented given the simpler linear-static options available.

While FBD boasts an attractive simplicity, Priestley (2003) and others pointed out several shortcomings. The use of displacement-based design (DBD) was thus advocated, where deformation demands in the individual elements drive the design process, culminating in the development of the direct displacement-based design (DDBD) method (Priestley et al. 2007) and other similar methods (Sullivan et al. 2003). One of the principal arguments by Priestley et al. (2007) was that it was not reasonable to quantify the expected ductility and spectral demand reduction for different structural configurations via unique behaviour factors and proposed employing a ductility and typology-dependant spectral reduction.

Both FBD and DBD methods can be good approximations for the initial seismic design of structures. However, neither explicitly quantify the structural performance in a manner that may be considered as having fully satisfied the goals of modern PBEE (i.e. the PEER PBEE methodology). This means that the actual performance of structures designed using these methods is not expected to be risk-consistent (i.e. the annual probability of it exceeding a certain performance threshold is not accurately known or consistent among different structures), and building performance parameters like collapse risk, expected economic losses and downtime do not feature in the design process. A recent initiative in Italy (Iervolino et al. 2018) has shown that buildings designed according to the Italian national code (NTC 2018), which is similar to EC8, do not exhibit the same level of collapse safety when evaluated extensively, with large variations observed between different structural typologies and configurations. These FBD and DBD methods' design solutions may be refined and modified to become more in-line with risk-based objectives, as discussed in O'Reilly and Calvi (2020), or the behaviour factors adopted for different structural typologies may

be adjusted and refined (Vamvatsikos et al. 2020), for example. Nevertheless, the fundamental issue of modern PBEE not being at the core of these classical methods remains.

2.2 Recent risk-targeted approaches

Over the years, different design methods aimed at risk-targeted have been developed and are widely accepted to eventually be prescribed and recommended in future design codes (Vamvatsikos et al. 2016; Fajfar 2018). The US has already implemented criteria in the seismic design code ASCE 7-16 (2016) and FEMA P-750 (2009b), and the new draft version of EC8 (CEN 2018) will include an informative annex on the probabilistic verification of structures. Any risk-targeted approach aims to control the risk of exceeding a limit state related to the performance of the building. Several methodologies to design structures with sufficient collapse safety are considered and are briefly mentioned before critically reviewed together with the proposed method in Sect. 4.

The concept of risk-targeted behaviour factors (RTBF) was developed based on the works of Kennedy and Short (1994) and Cornell (1996), whereby behaviour factors are adjusted and revamped using more risk-consistent approaches. Procedures like FEMA P695 (ATC 2009a) and recently by Vamvatsikos et al. (2020) outlined such approaches. Luco et al. (2007) introduced the concept of a risk-targeted design spectra to ensure uniform collapse risk for structures in the US. Douglas et al. (2013) and Silva et al. (2016) explored the extension of such an approach to Europe. Vamvatsikos and Aschheim (2016) further developed the yield point spectrum method by Aschheim and Black (2000) and introduced the yield frequency spectra (YFS) as a design aid to link the MAFE of any displacement or ductility-based parameter with the system design strength. Additionally, Žižmond and Dolšek (2019) introduced the risk-targeted seismic action method to be integrated with the current FBD procedures in EC8. Krawinkler et al. (2006) also introduced an iterative approach, where effective structural systems are selected and sized and the performance of structural, non-structural, and content systems is evaluated for each. This approach utilises acceptable loss and collapse risk for decision-making to intuitively aid designers when implementing the PEER PBEE framework in design. These aforementioned studies are not intended to be an exhaustive list of available methods but rather some of the noteworthy proposals to integrate modern PBEE in seismic design.

3 Proposed integrated performance-based seismic design (IPBSD)

3.1 Overview

A novel conceptual seismic design framework that employs expected annual loss (EAL) as a design metric and requires very little building structure information at the design outset was developed by O'Reilly and Calvi (2019) and forms the basis of the proposed approach. It centres around defining a limiting value of EAL and identifying structural solutions through simplified hand calculations. Several assumptions were made to relate the performance objectives to a design solution space, which serves as an initial screening before detailing the structural members. Storey loss functions (SLFs) were used to relate expected loss ratios (ELRs, γ) to engineering demand parameters (EDPs). A serviceability limit state (SLS) and ultimate limit state (ULS) were considered to

characterise the structure's elastic and ductile behaviour (Shahnazaryan et al. 2019), respectively, in line with current code prescriptions.

The proposed framework outlined herein uses mean annual frequency of collapse (MAFC), λ_c , to directly ensure an acceptable level of collapse safety and an EAL limit, $\lambda_{y,limit}$, to mitigate excessive monetary losses. Both are set by the designer based on the desired building performance. The target MAFC, $\lambda_{c,target}$, is set and used to limit the actual λ_c described by:

$$\lambda_c = \int_0^{+\infty} P[C|Sa(T)]|dH(Sa(T))| \leq \lambda_{c,target} \tag{2}$$

and the $\lambda_{y,limit}$ limits the λ_y described by:

$$\lambda_y = \int_0^{+\infty} E[y]|dH| \leq \lambda_{y,limit} \tag{3}$$

This integrated consideration of building performance in a risk-consistent manner represents a positive step for future revisions of design codes in line with the goals of modern PBEE.

3.2 Step-by-step implementation of the proposed IPBSD framework

A step-by-step guide to the proposed IPBSD framework is outlined herein. It is described with reference to an RC frame, although the framework may be extended to other structural typologies. It comprises four phases:

1. Definition of performance objectives (Fig. 1);
2. Identification of feasible initial period range (Fig. 2);
3. Identification of required lateral strength and ductility capacity (Figs. 3, 4);
4. Design and detailing of structural elements (Fig. 5).

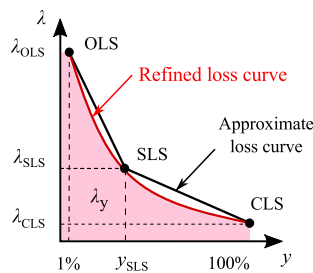


Fig. 1 Phase 1 of the proposed framework, where the loss curve is constructed and SLS performance objectives established to limit EAL

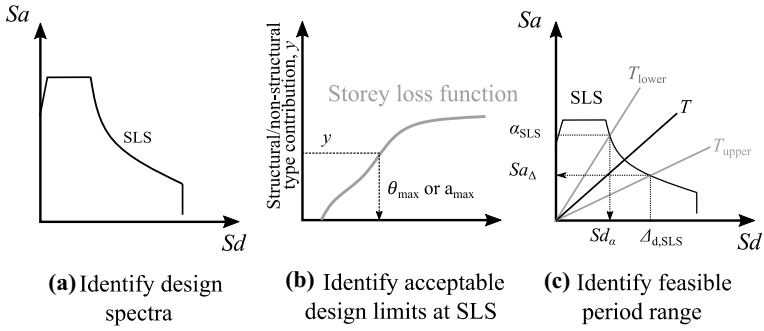


Fig. 2 Phase 2 of the proposed framework, where design spectrum and acceptable design limits at SLS are identified, leading towards the establishment of the feasible initial period range

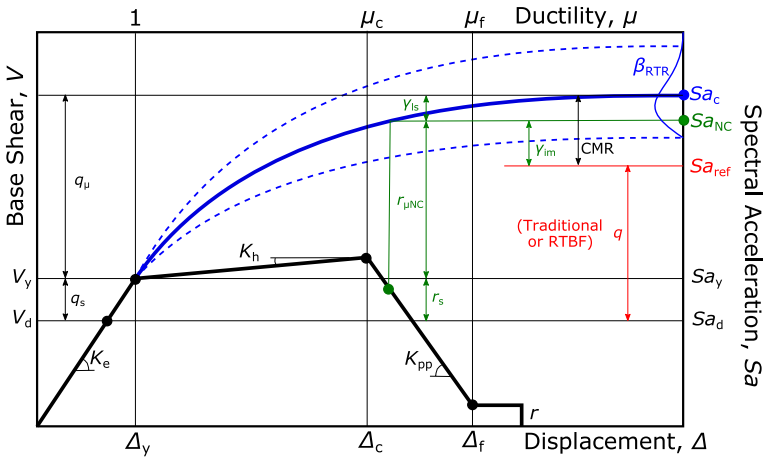


Fig. 3 Illustration of the SPO backbone response parameters and the various approaches to identify the design value

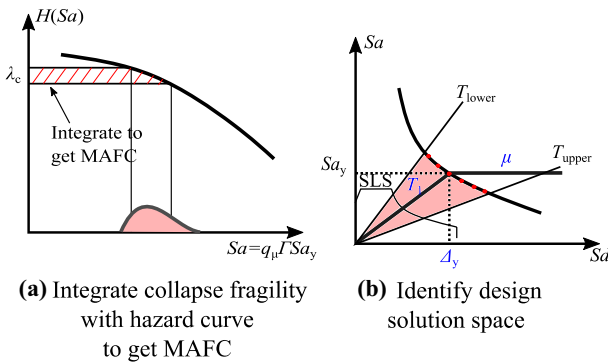


Fig. 4 Phase 3 of the proposed framework, where the collapse capacity and backbone curve of the solution is identified

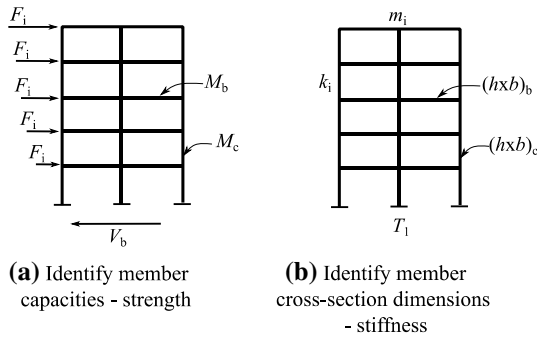


Fig. 5 Phase 4 of the proposed framework, where the demands on the structural elements are identified and detailing of sections is carried out

3.2.1 Phase 1: definition of performance objectives

In the first phase of IPBSD, the aim is to identify a suitable loss curve to limit λ_y . Performance objectives are characterised through an ELR, y , and MAFE, λ , of each limit state shown in Fig. 1. Three limit states utilised are: fully operational limit state (OLS), which represents the onset of damage and monetary loss and is assumed to be $y_{OLS} = 1\%$ at a limit state return period of 10 years; SLS, which is where the economic losses will be controlled through the modification of y_{SLS} ; collapse limit state (CLS), where complete collapse (i.e. $\lambda_{CLS} = \lambda_c$) and economic loss of the building (i.e. $y_{CLS} = 100\%$) is expected. With both the OLS and CLS known, a y_{SLS} and λ_{SLS} are assigned to SLS in Fig. 1 and the loss curve is identified. O'Reilly and Calvi (2019) have shown that the difference in area between the approximate and refined loss curve shown in Fig. 1 could be over 50%, resulting in a large overestimation of EAL. To overcome the overestimation, they suggested a closed-form fit for the refined loss curve as follows:

$$\lambda(y) = c_0 \exp[-c_1 \ln y - c_2 \ln^2 y] \tag{4}$$

where c_0 , c_1 and c_2 are the fitting coefficients for the three limit state points. The area under the curve (i.e. the red shaded area) is λ_y given by Eq. (5), where a trapezoidal rule may be applied and is checked against $\lambda_{y,limit}$ defined initially. SLS's characteristics, namely y_{SLS} and λ_{SLS} , are the variables to be adjusted so that λ_y is not exceeding $\lambda_{y,limit}$. The value of λ_{SLS} should be in line with current code requirements and the value of y_{SLS} be the parameter adjusted to satisfy Eq. (5).

$$\lambda_y = \lambda_{OLS} y_{OLS} + \int_{y_{OLS}}^{y_{CLS}} \lambda(y) dy \leq \lambda_{y,limit} \tag{5}$$

3.2.2 Phase 2: identification of a feasible initial period range

Phase 2 of the proposed framework identifies a range of possible initial structural periods $[T_{lower}, T_{upper}]$. Using the λ_{SLS} identified in Sect. 3.2.1, the design spectrum shown in Fig. 2a can be obtained through an appropriate anchoring of a design spectrum, characterised via PGA, that results in SLS exceedance. A second-order hazard model

(Vamvatsikos 2013) is used for the peak ground acceleration (PGA) of this spectrum and is given as:

$$H(s) = k_0 \exp(-k_1 \ln s - k_2 \ln^2 s) \tag{6}$$

where k_0, k_1, k_2 are the fitting coefficients, and $H(s)$ is the hazard function representing the MAFE of a certain intensity measure (IM), s , equal to PGA in this case, obtained from probabilistic seismic hazard assessment (PSHA). The hazard level corresponding to λ_{SLS} , is determined by solving for H_{SLS} in the following expression (Vamvatsikos 2013):

$$\lambda_{SLS} = \sqrt{p} k_0^{1-p} H_{SLS}^p \exp(0.5 p k_1^2 \beta_{SLS}^2) \tag{7}$$

$$p = \frac{1}{1 + 2k_2 \beta_{SLS}^2}$$

where β_{SLS} is the dispersion anticipated at the SLS, which could be taken as 0.20 and is within the bounds of the recommended values of Appendix F of the recent draft of the revised EC8 (CEN 2018). Knowing the hazard level, the PGA of SLS is calculated by simply inverting Eq. (6) as:

$$PGA = \exp \left[\left(-k_1 + \sqrt{k_1^2 - 4k_2 \ln \frac{H_{SLS}}{k_0}} \right) / (2k_2) \right] \tag{8}$$

and the uniform hazard spectrum (UHS) for SLS is obtained (Fig. 2a).

Control in the context of economic losses is established by limiting structural demands at the SLS. This means limiting displacement and acceleration demand on the structure for the design SLS spectrum identified. Using storey loss functions, acceptable structural demand limits are identified, as illustrated in Fig. 2b. As further described by O'Reilly and Calvi (2019), relative weights or contributions of different damageable groups to expected loss, Y , at the SLS are required. The ELR at SLS, y_{SLS} , is therefore broken down as:

$$y_{SLS} = y_{S,PSD} + y_{NS,PSD} + y_{NS,PFA} \tag{9}$$

comprising peak story drift (PSD) sensitive structural, $y_{S,PSD}$, and non-structural, $y_{NS,PSD}$, elements, and peak floor acceleration (PFA) sensitive non-structural, $y_{NS,PFA}$, loss contributions. These may be computed as a product of target y_{SLS} and its relative weighting Y by the following expressions:

$$y_{S,PSD} = y_{SLS} Y_{S,PSD}$$

$$y_{NS,PSD} = y_{SLS} Y_{NS,PSD} \tag{10}$$

$$y_{NS,PFA} = y_{SLS} Y_{NS,PFA}$$

By entering the vertical axis in Fig. 2b with the respective value of $y_{S,PSD}$ or $y_{NS,PSD}$, the more critical maximum PSD, $\theta_{max,SLS}$, and the maximum PFA, $a_{max,SLS}$ are obtained. These multi-degree of freedom (MDOF) demand limits are then converted to single-degree of freedom (SDOF) spectral displacement, $\Delta_{d,SLS}$ and spectral acceleration, $\alpha_{d,SLS}$ limits. Similar to the approach adopted in DBD (Priestley et al. 2007), the spectral displacement limit is computed as:

$$\Delta_{d,SLS} = \frac{\sum_{i=1}^n m_i \Delta_i^2}{\sum_{i=1}^n m_i \Delta_i} \tag{11}$$

$$\Delta_i = \omega_\theta \theta_{max,SLS} H_i \left(\frac{4H_n - H_i}{4H_n - H_1} \right) \tag{12}$$

where n is the number of storeys, m_i is the floor mass and Δ_i is the first mode-based displaced shape of the RC frame at storey level i , but other typologies can be considered (Priestley et al. 2007), ω_θ is the higher mode reduction factor and H_i is the i -th storey's elevation above the base. Unlike PSD, the maximum PFA along the height, a_{max} , cannot be assumed to be first-mode dominated. Here, a simplified assumption is made, where the transformation coefficient is assumed as 0.6, based on the findings of O'Reilly and Calvi (2019) (Eq. (13)). Further refinements have (Silva 2020) and are being currently been investigated for transformation coefficients of different structural typologies.

$$\alpha_{d,SLS} \approx 0.6 a_{max,SLS} \tag{13}$$

Based on these design spectral limits, a period range bounded by the lower, T_{lower} , and upper, T_{upper} , limits is identified (Eqs. (14) and (15)), within which the fundamental period of the structure, T_1 , must be (Fig. 2c). Having a structure whose period falls in this range should ensure that the building is neither too stiff, which would result in excessive floor acceleration-sensitive losses, nor too flexible, which would give excessive drift-sensitive losses, at the SLS. Meeting these conditions aims to ensure that the EAL limits discussed in Phase 1 are respected.

$$T_{lower} = 2\pi \sqrt{\frac{Sd_\alpha}{\alpha_{SLS}}} \tag{14}$$

$$T_{upper} = 2\pi \sqrt{\frac{\Delta_{d,SLS}}{S\alpha_\Delta}} \tag{15}$$

3.2.3 Phase 3: identification of required lateral strength and ductility

Having identified the feasible initial period range to limit economic loss at SLS, it is equally important to control the risk of structural collapse. Unlike the previous iteration of the framework (O'Reilly and Calvi 2019), the direct consideration of ULS is replaced with CLS, and a MAFC is targeted by Eq. (2). A period between T_{lower} and T_{upper} is selected and the expected backbone behaviour and overstrength q_s are first trialled by the designer. SPO parameters are assumed, such as the spectral acceleration at yield, Sa_y , the fundamental period T_1 , hardening and fracturing ductilities, μ_c and μ_f , hardening ratio to peak, K_h and post-peak softening ratio, K_{pp} , and residual strength, r (Fig. 3). For the initial estimation of these parameters, several suggestions from the literature may be employed. For example, μ_c may be initially estimated based on the behaviour factors given in current codes; μ_f will depend on the post-peak capping rotation capacity of the RC frame members, which could be based on work by Haselton et al. (2016), for example. An r value of around 10–20% of Sa_y and K_{pp} could be within a range of

20–30% to start, but both should be based on pushover analysis or experimental testing when available. All of these parameters may be adjusted based on expert judgement by the designer and since they are structural capacity proportions and should not be too challenging to estimate and quickly refine without any excessive analysis being required.

The SPO2IDA tool (Vamvatsikos and Cornell 2005) is used to estimate the collapse fragility function of the structure in terms of median collapse capacity, Sa_c , and record-to-record (RTR) uncertainty, β_{RTR} , assuming a lognormal distribution. In essence, the SPO2IDA tool offers a quick estimation of the incremental dynamic analysis (IDA) response (i.e. the blue curves in Fig. 3), which represent the intensities required to exceed displacement-based limit-states of a structure characterised by an SDOF system with a quadrilinear SPO curve (i.e. the black backbone curve shown in Fig. 3). It utilises R - μ - T relationship, developed through extensive dynamic analyses on SDOF oscillators (Vamvatsikos and Cornell 2005) and removes the need of performing multiple dynamic analyses on the trialled backbone behaviour. The identified backbone shape in Fig. 3 and a trialled lateral strength Sa_y is used to find the ductility-based force-reduction, q_μ and β_{RTR} , using the SPO2IDA tool as:

$$[q_\mu, \beta_{RTR}] = f(Sa_y, T_1, \mu_c, \mu_f, a_p, a_{pp}, r) \tag{16}$$

For proper evaluation of collapse capacity, through square-root-of-sum of squares (SRSS) combination, modelling (and possibly other types) uncertainty needs to be accounted for (Eq. (17)).

$$\beta_{total} = \sqrt{\beta_{RTR}^2 + \beta_{modelling}^2} \tag{17}$$

q_μ is transformed to the spectral acceleration Sa of the actual MDOF system using a transformation factor, Γ , as follows:

$$Sa_c = Sa_y q_\mu \Gamma \tag{18}$$

$$\Gamma = \frac{\sum_{i=1}^n m_i \varphi_i}{\sum_{i=1}^n m_i \varphi_i^2} \tag{19}$$

where φ is the fundamental mode shape, which can be taken as the normalised displaced shape (Eq. (12)). The collapse fragility function is then integrated with the hazard curve corresponding to the selected T_1 , $H(Sa(T_1))$, identified from PSHA and λ_c is computed (Fig. 4a) by Eq. (20). The λ_c computed from the trialled value of Sa_y and the assumed backbone shape is verified against $\lambda_{c,target}$. If the condition is met and the value is sufficiently close to the target, the designer may proceed. Otherwise, the trialled yield properties of the frame and/or ductility should be revised. By varying T_1 and repeating the process, a capacity curve of uniform collapse risk can be plotted in Sa versus Sd , which identifies where the feasible structural solutions are to be found (shaded in red in Fig. 4b). The red dots in Fig. 4b represent several feasible design solutions within the period range and with a strength capacity that satisfies the collapse safety criterion, meaning that any structure with the T_1 in this range and a lateral capacity on the curve should be sufficient.

$$\lambda_c = \sqrt{p}k_0^{1-p}H(Sa_c)^p \exp(0.5pk_1^2\beta_{total}^2) \leq \lambda_{c,target}$$

$$p = \frac{1}{1 + 2k_2\beta_{total}^2}$$
(20)

3.2.4 Phase 4: design and detailing of structural elements

The final phase (Fig. 5) uses the identified required capacity to size the structural elements. Design base shear, V_d , based on the identified Sa_y is given by Eq. (21), which depends on the first-mode effective mass, M^* (Eq. (22)) and the assumed value of system overstrength, q_s . It is necessary to include a reduction for the anticipated overstrength such that the resulting structure will have an actual yield strength of Sa_y and thus a collapse risk of λ_c , as anticipated by the performance objectives depicted in Fig. 3.

$$V_d = \frac{Sa_y}{q_s} M^* \Gamma$$
(21)

$$M^* = \sum_{i=1}^n m_i \varphi_i$$
(22)

Based on V_d the lateral distribution of forces may be obtained and is used to identify demands on structural elements, given as:

$$F_i = V_d \frac{m_i \Delta_i}{\sum_{i=1}^n m_i \Delta_i}$$
(23)

At this point, any structural member detailing requirement from seismic design codes may be applied to determine the member dimensions and required reinforcement content. Strength hierarchy and local ductility requirements should be accounted for. Of equal importance are higher mode effects and second-order effects (P-Delta). The former one may be accounted for through a higher mode reduction factor for the possible storey drift amplifications and P-Delta effects may be considered through stability checks similar to EC8 (CEN 2004b), for example. The structural element cross-section and material properties should be selected to remain within a reasonable tolerance of the assumed T_1 selected during the collapse safety verification phase. If this condition is met and the structure's capacity curve matches that of the assumed in Fig. 3, the identified structural configuration may be adopted. Otherwise, the element dimensions and reinforcement ought to be revised. It is noted, however, that any iterations required in IPBSD are limited to spread-sheet adjustments and extensive analysis verifications are not required.

4 Discussion of performance-based seismic design methods

With the brief overview of existing seismic design methods in Sect. 2 and the proposed method in Sect. 3, a critical discussion is provided here. Table 1 shows several designs method with the following abbreviations: IPBSD proposed here; FBD present in many seismic design codes (CEN 2004b; NZS 1170.5: 2004; ASCE 7-16 2016; NTC 2018); DDBD outlined by Priestley et al. (2007); RTBF described by Cornell (1996), amongst

Table 1 Comparison of key similarities and differences of available seismic design methods

	IPBSD	FBD	DDBD	RTBF	CPBD	RTS	YFS	RTSA-D	RTSA-I
PO	λ_c	$E[D/T_R]$	$E[D/T_R]$	CMR	$E[L/T_R]$	λ_c	λ_0	λ_c	λ_c
H	λ_y	$E[R/T_R]$	UHS	UHS	$P[C/T_R]$	UHS	λ_μ	$H(Sa(T_1))$	$H(Sa(T_1))$
NL	$H(Sa(T))$	UHS	UHS	UHS $H(AvgSa)$	$H(Sa(T_1))$	UHS	SPO2IDA	Assume r_s and μ_{NC} and calculate C_1 from IDA	$H(Sa(T_1))$ and UHS
	Assume μ and q_s and get q_μ from SPO2IDA	Traditional q factors	Equivalent viscous damping	Calibrated q factors	NLRHA	Traditional q factors		Assume r_s and calculate C_1 from IDA	Assume r_s and μ_{NC} and calculate C_1 from IDA (Equivalent q factor)
DD	Moderate	Easy	Easy	Easy	Very extensive	Easy	Moderate	Extensive	Extensive
FLX	Flexible	Limited	Flexible	Limited	Flexible	Limited	Flexible	Flexible	Flexible
PBEE	Yes	No	No	Yes	Yes	No	Yes	Yes	Yes

others; conceptual performance-based design (CPBD) proposed by Krawinkler et al. (2006) Zareian and Krawinkler (2012); risk-targeted spectra (RTS) proposed by Luco et al. (2007); YFS proposed by Vamvatsikos and Aschheim (2016); and the risk-targeted seismic action (RTSA) method comprising both the direct (D) and indirect (I) approaches by Žižmond and Dolšek (2019). This list is not intended to be exhaustive but instead attempts to give an overview of the prominent methods currently available in research and practice.

The rows of Table 1 list several categories common to each seismic design method. These are abbreviated and described as follows: performance objective(s) (PO), which describe the primary quantity that each design method targets, limits or bases itself upon; seismic hazard (H) definition, meaning how seismicity is characterised in the design process; non-linearity (NL) meaning how ductile structural behaviour is accounted for to adequately determine a suitable set of reduced design forces; relative difficulty and directness (DD) meaning how difficult (i.e. is the method feasible with just a spreadsheet or is extensive NLRHA required?) and direct (i.e. are multiple iterations required to obtain the final solution?) the method is; (PBEE) whether or not the method is risk-consistent; and the flexibility (FLX) of the method meaning how easy is it to tailor the design targets beyond what it has been developed for so far.

The first comparative point concerns the POs. Beginning with FBD, the PO is related to the expected (or average) values of displacement, D , and lateral resistance, R , at specified return period, T_R , intensities. This requires a designer to ensure sufficient lateral strength at very rare T_R events, whilst limiting the expected displacement at frequent T_R events. DDBD follows a similar approach whereby the expected level of displacement demand at multiple T_R levels is used. This is quite typical of design codes, whereby a series of intensity-based checks with corresponding limit states are stipulated for practitioners to follow and verify. This essentially stemmed from the early interpretation of PBEE in Vision 2000 (SEAOC 1995).

As research grew on probabilistic-related aspects, it became clear that such an intensity-based approach may not be entirely appropriate for modern PBEE (Günay and Mosalam 2013) and structures designed this way did not provide the consistent level of safety they were perceived to have (Iervolino et al. 2018). This led to developments on how these approaches may be improved but maintaining the same intensity-based approach familiar to practitioners. RTS, RTBF and RTSA-I are examples of such developments, where some *behind the scenes* adjustments are made to maintain the familiar intensity-based approach via a UHS while seeking to maintain risk-consistency among designs. They typically have collapse safety as their PO but differ slightly in their definitions of it. For example, to identify suitable behaviour factors to reduce the UHS in design, FEMA P-695 (ATC 2009a) employs a collapse margin ratio (CMR, see Fig. 3), whereas a recent proposal by Vamvatsikos et al. (2020) for Europe employed λ_c .

YFS provides a way to identify structures that can limit the MAFE of deformation-based quantities like storey drift, θ , or ductility, μ . CPBD was a proposal that was in some ways ahead of its time as many of the tools needed to feasibly implement it were either not available, or yet to be developed. It discussed using an array of POs in its formulation and made an effort to illustrate these quantities for designers to understand. Further development of this approach by Zareian and Krawinkler (2012) utilised a storey-based approach with POs being defined as expected losses and collapse probabilities at specified intensities. This is one of the few methods that has attempted to directly incorporate economic losses into its formulation, although the manner in which it was framed appeared rather tough to practically implement at the time. The last is the proposed IPBSD approach where the POs are the λ_c and the λ_y to target a certain collapse risk but also to limit the expected

economic losses over all intensities, as initially proposed by O'Reilly and Calvi (2019). It is seen that the collapse risk objective is in line with other methods but the relatively simple integration of EAL as a design variable makes it an attractive option. This was a key point highlighted by Krawinkler et al. (2006), stating that performance-based designs are not readily condensable to a single design parameter but multiple parameters that affect different facets of response; for example, should the building possess insufficient strength and ductility, its collapse safety may be inadequate, whereas should it be too flexible, it may accumulate excessive drift-sensitive loss at low T_R events, but at the same time potentially accumulate too much acceleration-sensitive if too stiff. It was for this reason that O'Reilly and Calvi (2019) introduced the restriction of the initial period range and the subsequent identification of sufficient lateral strength and ductility.

The next broad comparison is the manner in which they define seismic hazard. Traditional methods like FBD and DDBD rely on the use of a UHS at specified T_R levels. These UHS are anchored to some level of ground shaking computed using PSHA. In the case of EC8, PGA on rock is used and a predefined shape for all other periods at that T_R is fitted. It should be noted that while the use of specific T_R levels may not be ideal, neither is anchoring the shape of the entire design spectrum to a single parameter like PGA, as recently discussed by Calvi et al. (2018). The main problem with using a UHS is that in order to make the resulting design solutions risk-consistent, they need to either have some modifications made in how they are utilised or how they are defined. For example, RTS attempts to define the anchoring value of a UHS whereas RTSA-I instead modifies how the force reduction is introduced. Alternatively, there is the use of seismic hazard curves determined from suitable PSHA, and are generically defined as $H(IM)$, noting that different IMs may be used. The most common hazard curve definition is at the first mode period of vibration of the structure, $H(Sa(T_1))$, which is employed by YFS, RTSA-D, RTSA-I and also IPBSD. The proposed method utilises several hazard curves defined within a range of feasible periods of vibration and not one specific value giving a degree of flexibility of final structural configuration when identified and sized. Other methods focus on the identification of a singular T_1 assumption for design which needs to be then iterated should the actual value not match. It is also noted how the RTBF quantification approach described by Vamvatsikos et al. (2020) for Europe utilises a more advanced IM definition of average spectral acceleration (Eads et al. 2015), $H(AvgSa)$, to characterise suitable behaviour factors.

In terms of how each method deals with non-linearity, FBD uses the traditional approach of behaviour factors for each structural system whereas other methods like RTBF have attempted to correct the definition of these to be more risk-consistent. However, the underlying assumption of a single force reduction factor for certain typologies remains. RTS as defined in ASCE 7-16 (2016) also utilises force reduction factors but as pointed out by Gkimprxis et al. (2019), this use of traditional behaviour factors means that the risk-consistency breaks down in this implementation of RTS. The RTBF approach attempts to rectify this inconsistency through appropriate behaviour factor calibration. DDBD utilises the concept of equivalent viscous damping, which is somewhat similar to behaviour factors but different because the spectral reduction is a function of the expected ductility demand rather than a fixed value. CPBD utilised a rather strenuous approach of multiple NLRHA for identification of suitable designs. The RTSA methods proposed by Žižmond and Dolšek (2019) account for non-linearity by assuming a set of values for the expected ductility capacity at near collapse, μ_{NC} , and over-strength of the structure, r_s , which are later verified for the subsequent design and iterated if needed. An additional C_1 parameter is also computed via an IDA analysis on an equivalent SDOF oscillator. It is worth noting that for the RTSA-I method, Žižmond and Dolšek (2019) describe how an equivalent risk-consistent behaviour factor may be identified, highlighting

the link between it and other methods discussed here. To circumvent the use of assumed values for force reduction and subsequent verification, YFS and the proposed IPBSD method both utilise the SPO2IDA tool (Vamvatsikos and Cornell 2005) to compute the force reduction distribution directly. This tool relates the distribution of dynamic behaviour to the expected backbone shape of the structure using an extensive library of empirical coefficients calibrated using NLRHA. This has the advantage of allowing the dynamic behaviour to be estimated with a high degree of accuracy prior to designing the structure without any numerical analysis.

Regarding the relative difficulty and directness of each method, a generic ranking has been provided based on the authors' subjective opinion. Due to their direct nature and no essential requirement to iterate design solutions or conduct extensive dynamic verifications, the FBD, DDBD, RTBF and RTS methods are ranked as easy methods to implement. The CPBD method is ranked as very extensive due to the sheer amount of analysis required to implement it. The YFS and IPBSD methods are ranked as moderate as they do not require any dynamic analysis to implement. If the designer is confident in SPO2IDA tool's ability to characterise the dynamic behaviour of the structure then no great difficulty is encountered. Small iterations may be needed to refine the solution, with some being refined to a spreadsheet whereas others require pushover analysis of numerical models. The RTSA methods are denoted as extensive by requiring an IDA on an SDOF oscillator to determine one of the design parameters. Designs may take a few iterations, with full numerical models being required. The authors of this approach have, to their credit, provided ample parametric studies and practical guidance for designers (Sinković et al. 2016) on how to tackle this aspect and good initial assumptions can easily be made, still making it an attractive option.

In terms of flexibility of tailoring the design targets, the methods using behaviour factors (FBD and RTBF) are relatively limited since their performance is inherently linked to the assumption made in the derivation of the behaviour factor and no end-control is left to the designer. DDBD's use of equivalent viscous damping makes it somewhat more flexible as it allows designers to tailor their intensity-based drift limitations. The assumptions needed to derive RTS have been discussed by Gkimprixis et al. (2019) to not be without their difficulties as to how the general method ought to be employed and the spectra derived with different studies advocating different anchoring values of the parameter X (Douglas et al. 2013; Silva et al. 2016). All other methods are deemed as flexible as they let designers choose and tailor their specific design targets, increasing their appeal.

Lastly, Table 1 categorises the different methods as being PBEE-compliant or not. While this is not a new discussion (e.g. Vamvatsikos et al. 2016), it is included here for completeness. Unsurprisingly, neither FBD nor DDBD meet modern PBEE goals, at least without some additional verifications (e.g. O'Reilly and Calvi 2020). Again, RTS fails this categorisation not because of a conceptual flaw but rather in how it has come to be implemented, as discussed by Gkimprixis et al. (2019). The other methods, including the proposed IPBSD, are all seen to be PBEE-compliant as their formulations directly incorporate the use of risk-oriented metrics implemented consistently.

5 Case study application

5.1 Definition of case study buildings

To assess the performance of the existing methods compared to the proposed one, several case study applications were carried out. Ten archetypical buildings were examined

Table 2 Archetypical RC frame structures

Case	$\lambda_{c,target}$	$\lambda_{y,limit}$ (%)	Storeys		Bays	
			# Storeys	Ground storey/typical storey height (m)	# Bays	Width (m)
1	5.0×10^{-4}	0.65	2	3.5/3.0	2	5.0
2	1.0×10^{-4}	0.65	2	3.5/3.0	2	6.0
3	5.0×10^{-4}	0.65	4	3.5/3.0	3	Internal: 2.0 External: 4.5
4	1.0×10^{-4}	0.65	4	3.5/3.0	3	Internal: 2.0 External: 4.5
5	5.0×10^{-4}	0.65	4	3.5/3.0	3	6.0
6	1.0×10^{-4}	0.65	4	3.5/3.0	3	6.0
7	5.0×10^{-4}	0.45	6	3.5/3.0	3	Internal: 2.0 External: 4.5
8	1.0×10^{-4}	0.45	6	3.5/3.0	3	Internal: 2.0 External: 4.5
9	5.0×10^{-4}	0.45	8	3.5/3.0	3	Internal: 2.0 External: 4.5
10	1.0×10^{-4}	0.45	8	3.5/3.0	3	Internal: 2.0 External: 4.5

and are described in Table 2. The designs vary in terms of number of storeys, number of bays, storey heights and bay widths, in addition to design targets. Office occupancy was assumed for each and the SLFs provided by Ramirez and Miranda (2009) for this occupancy type were selected.

The value of λ_y was selected to a rating higher than “A” as classified by Cosenza et al. (2018) with values lower than 1%. As pointed out by Cook et al. (2019), damage in high-rise structures tends to concentrate on just a few storeys, greatly reducing the loss with respect to the total building value. In contrast, damage in shorter structures tends to be more spread across all storeys. Additionally, Ramirez et al. (2012) and Calvi et al. (2014) noted a trend whereby increasing building height results in decreasing normalised loss ratios and EAL. From this, one could argue that for taller structures, the λ_y is expected to reduce, hence the reduction of the limiting value for the taller case studies examined here. With regards to the selection of $\lambda_{c,target}$, there is yet to be a widespread consensus on which value should be used in new design. For example, ASCE 7-16 (2016) has an acceptable national risk of 1% in 50 years ($\lambda_c = 2.0 \times 10^{-4}$), while several studies from the literature (e.g. Duckett 2004; Goulet et al. 2007; Fajfar and Dolšek 2012) note values of around $\lambda_c = 1.0 \times 10^{-5}$ as reasonable. Furthermore, Silva et al. (2016) utilised $\lambda_c = 5.0 \times 10^{-5}$ whilst discussing the development of risk-targeted hazard maps for Europe and a review by Dolšek et al. (2017) noted typical limits are between $\lambda_c = 10^{-4}$ and 10^{-5} . Using these values from the literature, and also to highlight the possibility of easily tailoring the design performance objectives in the proposed method, two $\lambda_{c,target}$ values of 5.0×10^{-4} and 1.0×10^{-4} were adopted.

Typical plan and elevation illustrations are shown in Fig. 6. The gravity loads, including imposed and dead loads, were assumed 6 kN/m² and 5 kN/m² at the general floor and roof level, respectively. A stiff clay site according to EC8's site classification (CEN 2004b) located in L'Aquila, Italy was chosen for all design cases. The structural system

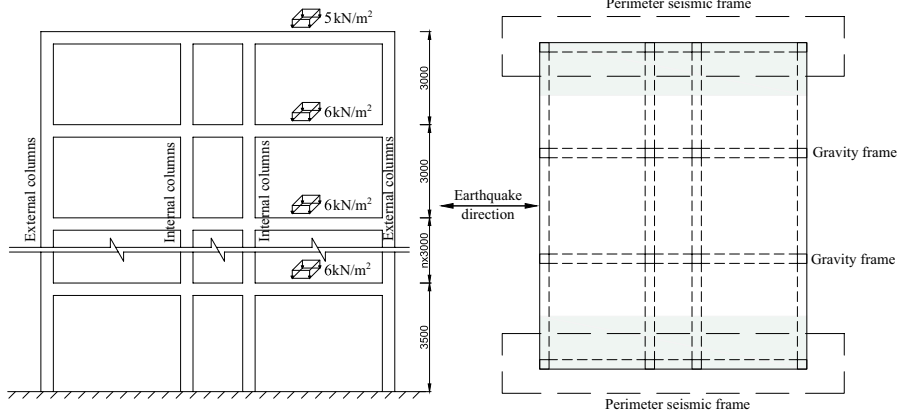


Fig. 6 Illustration of plan layout and elevation of archetypical RC frames in a discussion (tributary area of gravity loads on seismic frames shaded grey)

was a RC moment-resisting frame. The material properties used in the design and detailing were 25 MPa for the concrete compressive strength and 415 MPa for the steel yield strength. No plan or elevation irregularities were considered. 2D planar models were used given the symmetric structures with no irregularities. Alternatively, the framework should be applied in both directions of the structure bearing in mind that some considerations need to be applied for calculation of losses, which are not addressed herein. For simplicity, one direction of seismic action was considered.

5.2 Numerical modelling

For each design method and case study archetype, numerical models of the systems were generated using OpenSees (McKenna et al. 2010; Mazzoni et al. 2006) for subsequent design verification. SPO and NLRHA were performed to assess the seismic performance of each case. The masses were lumped at each floor and the nodes were constrained in the horizontal

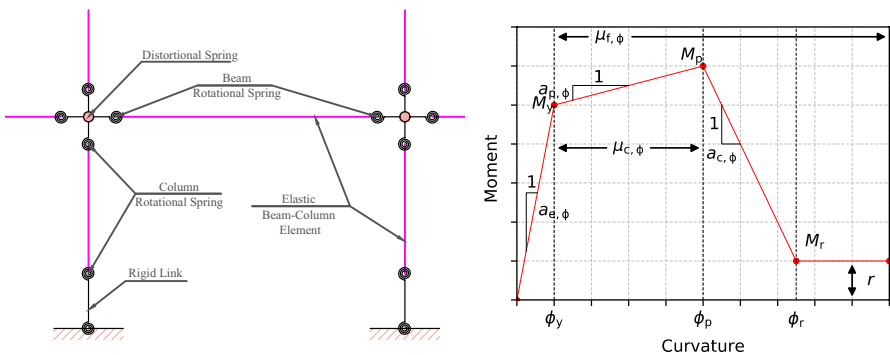


Fig. 7 Illustration of the numerical modelling approach, where (left) shows the layout of elements and beam-column connection modelling and (right) denotes the hysteretic model adopted for each hinge location

direction to mimic a rigid diaphragm behaviour (Fig. 7a). Non-linear element behaviour was considered through a concentrated plasticity approach developed by Ibarra et al. (2005) (Fig. 7b). P-Delta effects were accounted for through gravity columns, and the columns of the lateral force-resisting system were fixed at the base. Rayleigh damping was implemented with 5% of critical damping assigned to the first and third modes. For the plastic hinge models, element moment–curvature relationships were attained through Response-2000 sectional analysis program (Bentz 2015), which followed the concrete and reinforcement material properties of EC2 (European Committee for Standardization (CEN) 2004a). The backbone curve used is described by the parameters: elastic stiffness defined through the elastic slope, $a_{c,\phi}$, yield strength, M_y , yield curvature, ϕ_y , strain-hardening stiffness through hardening slope, $a_{p,\phi}$, capping curvature, ϕ_p , defined through hardening ductility, $\mu_{c,\phi}$, which corresponds to the peak strength, M_p , of the load–deformation curve. The softening branch is defined by the post-capping stiffness defined through softening slope, a_c . Finally, a residual strength, r , of the component is defined, which is preserved once a given deterioration threshold, ϕ_r , is achieved. The fracturing ductility, $\mu_{f,\phi}$, is used to identify a point of fracturing identifying a curvature capacity of the model. Essentially, the backbone curve was fit to the moment–curvature relationship of the element, where μ_c was selected based on the peak behaviour of the element and r was taken as 20% of M_y . The softening slope of the backbone curve was selected, so that the post-capping chord rotation capacity did not exceed 0.10, as per Haselton et al. (2016); the post-capping curvature capacity, ϕ_{pc} , may be obtained by taking the ratio of this to the anticipated plastic hinge length, L_p , calculated as per (Priestley et al. 2007), for example.

5.3 Site hazard and ground motions

PSHA was performed using OpenQuake (Pagani et al. 2014) with the SHARE hazard model (Woessner and Wiemer 2005). To characterise the structural response with increasing intensity for each design case, a set of 30 ground motion records were selected from the NGA West-2 database (Ancheta et al. 2014) with each record's soil type being consistent with that of the site. PSHA disaggregation results at the 2475 years return period and at a period of 0.7 s, around which the majority of the case study RC frames' T_1 fell, were used to select the records. Hazard curves obtained from PSHA were used in each design procedure under consideration. For the proposed framework, the initial definition of a target loss curve and identification of a suitable PGA value for the SLS was needed. Furthermore, once the acceptable period range for the structure was identified, $\lambda_{c,target}$ was verified by integrating the collapse fragility with the seismic hazard based on an IM of $Sa(T_1)$ for a range of T_1 values. Žižmond and Dolšek (2019), on the other hand, use a 1st order fit of $Sa(T_1)$ using the return periods of 475 and 10,000 years. The slope of the first-order model in the log–log domain was used to calculate the collapse intensity and the risk-targeted design spectral acceleration. For EC8 and DDBD cases, an elastic design spectrum was used. To be consistent with the seismic hazard used for the other methods, the $Sa(T_1)$ value of the elastic design spectrum defined was scaled to match that obtained from PSHA. This essentially meant that the EC8 design spectrum was anchored to a hazard consistent value of $Sa(T_1)$ rather than PGA on rock, as is typically recommended. The seismic hazard corresponding to a period of 0.7 s and 1.0 s are presented in Fig. 8. For the 2nd order hazard, least-squares fitting was used with higher weight given to medium to higher intensities, i.e. larger than $Sa(T) = 0.1$ g, where the collapse behaviour is more relevant for capturing λ_c , while for PGA intensity, higher weight was given to lower to medium intensities, where λ_y calculation is more relevant.

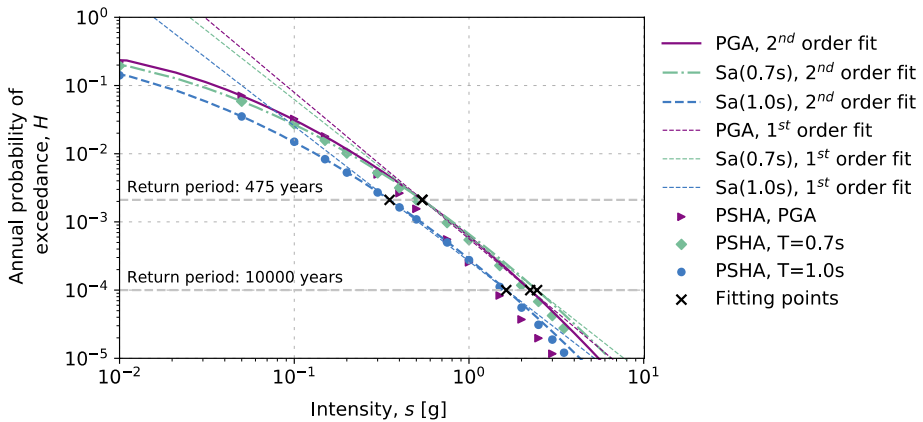


Fig. 8 Seismic hazard with 1st and 2nd order fits corresponding to a spectral acceleration at a period of 0.7 s, 1.0 s and PGA

6 Design of case study structures

The study aims to examine different methodologies for designing structures described in Sect. 5.1. In this section, the proposed IPBSD was implemented in addition to FBD as outlined in EC8, RTSA-D and RTSA-I by Žižmond and Dolšek (2019); the RTS approach by Luco et al. (2007) and DDBD as per Priestley et al. (2007). The RTBF, CPBD and YFS approaches were not applied here mainly in the interests of space but also for the following reasons. RTBF represents a general approach to update and correct behaviour factors used in design and to the authors' knowledge, none have been formally proposed for RC frame structures in Europe which would have allowed implementation here, although the studies previously discussed in Sect. 4 have indicated how they may be computed in future studies. CPBD was not studied here due to the sheer amount of analysis and iteration required to apply it. It was noted in Sect. 4 that one difficulty of CPBD was that it lacked the simplified tools to practically implement it. In this regard, the proposed IPBSD may be seen as a successor to this method, as the design objectives are similar but much of the heavy analysis work has been substituted with appropriate simplifications and tools for a more expedite design process. Lastly, YFS was also not considered because, if its performance objectives were changed from exceedance rates of multiple drift- and ductility-based conditions to the global collapse condition, the results would closely resemble those from Phase 3 of the proposed IPBSD method.

The objective was to examine contemporary methods of risk-consistent design in addition to code-based formulations. The RTS and DDBD approaches were examined up to the point of establishing a design strength and how it varies with respect to the other methods in the interest of space limitations. The same general approach to design was followed for each structure with the required lateral design strength identified and designed for. The case study structures were subsequently detailed and sized following the EC8 and EC2 member detailing requirements and a numerical model was built using the approach described in Sect. 5.2, to be evaluated in Sect. 7.

6.1 FBD according to EC8

The archetypical RC frames described in Table 2 were designed following the EC8 provisions. The design response spectrum provided by EC8 was used and scaled to match the $Sa(T_1)$ value from the PSHA at the no-collapse return period of 475 years. Since EC8 does not utilise λ_c in its design formulation, the values of $\lambda_{c,target}$ specified in Table 2 were not considered directly. To distinguish between buildings with differing levels of safety, EC8's importance classes were utilised. Therefore, buildings with $\lambda_{c,target} = 5.0 \times 10^{-4}$ and 1.0×10^{-4} were taken here approximately corresponding to importance classes II and III and the design spectrum was subsequently scaled by 1.0 and 1.2 to account for this, respectively.

The ELF method of analysis was employed to determine the demands on the structural elements and two sets of designs were considered: with and without the consideration of the gravity load combination. This was done to clearly identify the level of safety strictly provided by the ELF method's design resistance. Lateral drift limitations and P-Delta effects were satisfied and the member reinforcement content and dimensions were selected to be within the recommended local ductility limits for ductility class medium (DCM) frames. Cracked cross-section properties (i.e. 50% of gross) were used to identify the demands and design the structural elements. Adequate strength hierarchy (i.e. capacity design) requirements were also met. The period of the frames was identified via an iterative design procedure, where an initial $T_1 = 0.7$ s to match the period of the hazard curve was used. If this assumption was not satisfied and element cross-section properties needed revisions, T_1 was updated. The final design values are listed in Table 3.

Table 3 Summary of the design solutions obtained using FBD according to EC8, where G indicates cases where the gravity load combination was included

Case	Importance class	T_1 (s)	Sa_d (g)
1	II	1.1	0.10
1-G	II	1.1	0.16
2	III	1.1	0.11
2-G	III	0.7	0.27
3	II	2.3	0.04
3-G	II	1.3	0.13
4	III	2.3	0.05
4-G	III	1.1	0.15
5	II	1.8	0.06
5-G	II	1.3	0.14
6	III	1.8	0.07
6-G	III	1.3	0.16
7	II	2.3	0.05
7-G	II	1.8	0.08
8	III	2.3	0.05
8-G	III	1.8	0.09
9	II	3.0	0.03
9-G	II	2.5	0.06
10	III	3.0	0.04
10-G	III	2.5	0.07

Table 4 Summary of the design solutions obtained using DDBD according to Priestley et al. (2007)

Case	Importance Class	T_1 (s)	Design μ	Sa_d (g)
1	II	0.7	2.2	0.12
2	III	0.7	2.2	0.17
3	II	0.7	3.6	0.05
4	III	0.7	3.6	0.08
5	II	1.0	2.0	0.06
6	III	1.0	2.0	0.09
7	II	0.7	3.3	0.06
8	III	0.7	3.9	0.07
9	II	0.9	2.4	0.06
10	III	0.9	2.9	0.07

6.2 DDBD

The design cases of Table 2 were designed using DDBD (Priestley et al. 2007) and are presented in Table 4. The aim was to have a comparative basis among the design spectral accelerations between different methods of design. Similar to FBD, the values of $\lambda_{c,target}$ specified in Table 2 were not directly incorporated and EC8 importance classes were considered instead.

The same elastic spectrum was utilised and scaled to match the $Sa(T_1)$ of the seismic hazard. ASCE 7-16 (2016), for example, provides drift limit of 4% to 5% depending on the number of storeys, while Gokkaya et al. (2016) suggest a more stringent value of 3% at MCE intensity level. Taking into consideration the T_R of 2475 years of MCE and T_R of 475 years used here, the drift limit was assumed to be 2.5%. The Sa_d values in Table 4 appeared slightly higher to the ones obtained via the FBD approach in Table 3. The design μ , were generally lower than the ones used when designing the EC8 cases. Consequently, this will have compensating effects towards slightly higher Sa_d .

6.3 RTSA method

The next approach considered was the RTSA method proposed by Žižmond and Dolšek (2019) and both RTSA-D and RTSA-I formulations were employed. Since the approach is risk-targeted, it is more in line with design objectives (e.g. $\lambda_{c,target}$). Following the method's step-by-step formulation, the risk-targeted design spectral acceleration, Sa_d , was estimated.

Scenarios following the RTSA-D formulation were subdivided into two subcases based on the assumption of the r_s and μ_{NC} to the no-collapse (NC) limit state, which are illustrated in Fig. 3. Cases A considered $r_s = 1$ and $\mu_{NC} = 3$, whereas cases B considered $r_s = 2$ and $\mu_{NC} = 6$; the latter pair correspond to those used in the design example by Žižmond and Dolšek (2019). Case A values were selected to be more in line with the structural capacity in the absence of any additional gravity load consideration or significant overstrength. Additionally, an initial choice of T_1 is needed for both formulations. Where this assumed period substantially differed to the numerical model, it was updated and the design recomputed for all RTSA-D cases but only some RTSA-I cases. These different combinations are listed in Table 5.

Table 5 Summary of the RTSA design solutions using the direct and indirect formulations for cases A ($r_s=1, \mu_{NC}=3$) and B ($r_s=2, \mu_{NC}=6$), where T indicates period updating

ID			$\lambda_{c,target}$	T_1 (s)		Sa_d (g)	
	Case	RTSA-D		RTSA-I	RTSA-D	RTSA-I	RTSA-D
1	TA	A	5.0×10^{-4}	0.70	0.70	0.36	0.43
	TB	TA		0.90	0.70	0.07	0.43
2	TA	A	1.0×10^{-4}	0.50	0.42	0.91	1.69
	TB	TA		0.74	0.35	0.17	1.13
3	TA	A	5.0×10^{-4}	0.70	0.90	0.39	0.51
	TB	TA		1.57	0.87	0.05	0.38
4	TA	A	1.0×10^{-4}	0.66	0.50	0.72	0.88
	TB	TA		1.10	0.50	0.16	0.85
5	TA	A	5.0×10^{-4}	1.00	1.06	0.30	0.27
	TB	TA		1.70	1.10	0.04	0.24
6	TA	A	1.0×10^{-4}	0.96	0.74	0.52	0.57
	TB	TA		1.04	0.74	0.15	0.91
7	TA	A	5.0×10^{-4}	0.74	1.11	0.48	0.43
	TB	TA		1.92	1.09	0.03	0.25
8	TA	A	1.0×10^{-4}	0.70	0.56	0.80	0.98
	TB	TA		1.66	0.57	0.08	1.20
9	TA	A	5.0×10^{-4}	0.95	1.06	0.34	0.31
	TB	TA		3.50	1.12	0.01	0.27
10	TA	A	1.0×10^{-4}	0.77	0.76	0.81	0.78
	TB	TA		3.46	0.76	0.02	0.78

For both formulations, $\lambda_{c,target}$, was set and the seismic hazard described in Sect. 5.3 was used depending on T_1 . The value of design spectral acceleration, Sa_d (Fig. 3), was determined by setting β_{RTR} to the suggested value of 0.4 and identifying a median collapse intensity, Sa_C , that satisfied $\lambda_{c,target}$ when integrating in Eq. (2). An acceptable median spectral acceleration for the NC limit state, Sa_{NC} , was calculated as the ratio between Sa_C and the limit-state reduction factor, γ_{ls} , taken from Dolšek et al. (2017) as 1.15. Sa_d was determined using the reduction factor, r_{NC} , as illustrated in Fig. 3, where r_{NC} was determined by:

$$r_{NC} = \frac{\mu_{NC}}{C_1} r_s \tag{24}$$

where C_1 is the inelastic deformation ratio relating the inelastic and elastic deformation at Sa_{NC} . To compute C_1 , an SDOF oscillator model with equivalent period and first mode mass was required and analysed with the aforementioned set of ground motions using IDA, as suggested by Žižmond and Dolšek (2019).

RTSA-I cases use a risk-targeted safety factor, γ_{im} , (Dolšek et al. 2017) given by:

$$\gamma_{im} = \frac{1}{\gamma_{ls}} (T_R \cdot \lambda_c)^{-\frac{1}{k}} \cdot \exp \left[\frac{k\beta_{RTR}^2}{2} \right] \tag{25}$$

where k is the slope of the 1st order hazard function in the log–log domain (Fig. 8). The risk-targeted reduction factor, q_a , used in this formulation was then computed from:

$$q_a = \frac{r_{NC}}{\gamma_{im}} \tag{26}$$

For the reference seismic design action, Sa_{ref} , a return period of 475 years was assumed and the $Sa(T_1)$ was divided by q_a to give Sa_d . The design spectrum was then obtained by normalising the EC8 elastic spectrum to Sa_d to implement the RMSA. Both formulations involved an iteration based on the modification of T_1 and cross-sections and re-running of the SDOF model to identify the C_1 ratio.

Contrary to RTSA-I cases, where results were generally consistent, the design solutions obtained for the RTSA-D cases exhibited some atypical values (Table 5). This was particularly true for the increase in the assumed values of r_s and μ_{NC} in cases B, which resulted in lower design demands on the structural elements. These high r_s and μ_{NC} values led to a higher value of r_{NC} , as per Eq. (24), which resulted in much lower Sa_d , as illustrated in Fig. 3. Conducting elastic analysis on a structural model with this lower design demand led to subsequent iterations of structural element dimension reductions in order to meet the local member ductility requirements. This in turn increased the T_1 of the structure, as seen for cases 9 and 10 of RTSA-D TB, for example. This highlights the importance not only of strength and ductility in design but also of sufficient stiffness for lateral systems.

6.4 Proposed IPBSD formulation

The proposed IPBSD framework presented in Sect. 3.2 was implemented and detailed following the EC8 and EC2 provisions. To illustrate, a single design scenario (Case 4) was selected and is described step-by-step herein. It is recalled that $\lambda_{c,target}$ and $\lambda_{y,limit}$ were 1.0×10^{-4} and 0.65%, respectively.

The first phase of the framework involved the definition of performance objectives following Sect. 3.2.1. The y values of OLS and CLS were fixed to $y_{OLS} = 1\%$ and $y_{CLS} = 100\%$, respectively, and λ_{OLS} was set as to correspond to a limit state return period of 10 years and $\lambda_{CLS} = \lambda_{c,target}$, respectively. The SLS parameters were then identified by first setting the $y_{SLS} = 6\%$, and trialling $\lambda_{SLS} = 2.07 \times 10^{-2}$. With these limit state values and resulting loss curve shown in Fig. 9a, the λ_y was calculated from the refined loss curve using Eq. (5) as

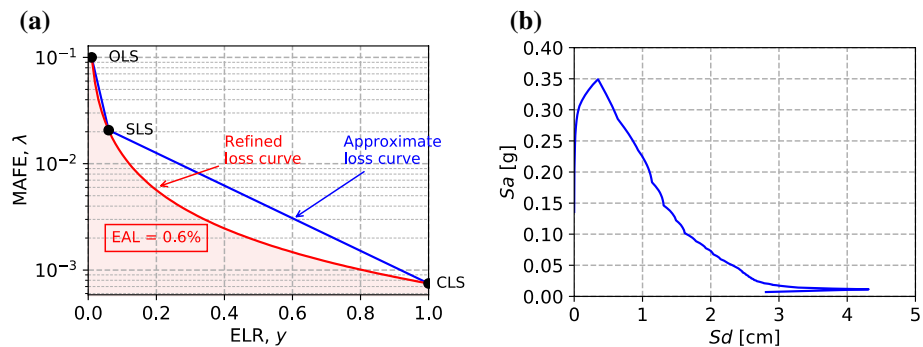


Fig. 9 a Loss curve and b design spectrum at SLS of design case 4

0.65%, corresponding to the limiting value. This choice of SLS parameters requires dedicated attention and further refinement beyond the scope of this work.

In phase 2, using λ_{SLS} the design spectrum at SLS was identified as per Sect. 3.2.2. β_{SLS} was defined as 0.2 and the hazard fitting coefficients were $k_0=365 \times 10^{-6}$, $k_1=2.043$, $k_2=0.155$. The PGA was identified as 0.136 g using Eqs. (6)–(8), based on which a design spectrum at SLS was identified (Fig. 9b) for the identification of a feasible initial period range. Then, the structural and non-structural loss contributions associated with each EDP were examined and limited based on the y_{SLS} previously identified. The SLFs proposed by Ramirez and Miranda (2009), assuming office occupancy for mid-rise structures were adopted (Fig. 10). For simplicity, the loss was assumed to be equally distributed along the height of the building and the relative contributions of the different loss groups, Y , were taken from the relative contributions of each SLF shown in Fig. 10. Given that the summation of each contribution exceeds 100% (Eq. (27)), the ELR associated with the element groups were normalised as shown in Sect. 3.2.2.

$$\begin{aligned}
 Y &= Y_{S,PSD} + Y_{NS,PSD} + Y_{NS,PFA} = 0.178 + 0.545 + 0.402 = 1.125 \\
 Y_{S,PSD} &= Y_{S,PSD} y_{SLS} = \frac{0.178}{1.125} \cdot 6\% = 0.95\% \\
 Y_{NS,PSD} &= Y_{NS,PSD} y_{SLS} = \frac{0.545}{1.125} \cdot 6\% = 2.91\% \\
 Y_{NS,PFA} &= Y_{NS,PFA} y_{SLS} = \frac{0.402}{1.125} \cdot 6\% = 2.14\% \\
 y_{SLS} &= y_{S,PSD} + y_{NS,PSD} + y_{NS,PFA} \\
 &= 0.95\% + 2.91\% + 2.14\% = 6.00\%
 \end{aligned}
 \tag{27}$$

Figure 10 presents how limiting EDPs were evaluated. For the PSD-sensitive elements, the most critical one was identified as the non-structural elements with a $\theta_{max}=0.42\%$ (Fig. 10b). For the PFA-sensitive non-structural elements, a_{max} was calculated as 0.49 g (Fig. 10c). Following Sect. 3.2.2, the spectral limits for PSD and PFA were computed as $\Delta_{d,SLS}=3.2$ cm and $\alpha_{d,SLS}=0.29$ g from Eqs. (11) and (13), respectively. Sd_α and Sa_Δ were retrieved from the SLS spectrum (Fig. 9b) corresponding to the design spectral values and the period range bounds were calculated based on Eq. (14) and (15) as follows:

$$T_{lower} = 2\pi \sqrt{\frac{Sd_\alpha}{\alpha_{SLS}}} = 6.28 \sqrt{\frac{0.61 \text{ cm}}{0.29 \cdot 981 \text{ cm/s}^2}} = 0.3 \text{ s}
 \tag{28}$$

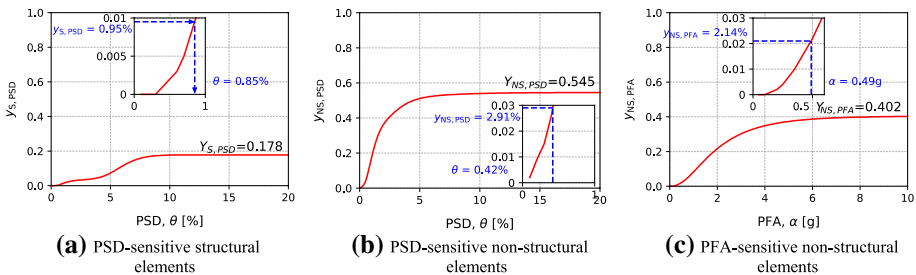


Fig. 10 Utilisation of the SLFs adopted from Ramirez and Miranda (2009)

$$T_{upper} = 2\pi \sqrt{\frac{\Delta_{d,SLS}}{Sa_{\Delta}}} = 6.28 \sqrt{\frac{3.2 \text{ cm}}{0.014 \cdot 981 \text{ cm/s}^2}} = 3.0 \text{ s} \quad (29)$$

A $T_1=0.9$ s, within the identified period range, was selected as the initial target period of the structure. By ensuring the structure has an initial period in this range, the EAL is expected to be lower than the predefined EAL limit. It is noted that the period range is relatively large, and is due to the level of hazard and limiting loss at SLS not being critical with respect to each other. Had a stricter EAL limit been imposed, the spectral limits would have reduced and the feasible period range would have tightened; likewise, had the seismicity increased and the SLS spectra ‘grown’ outwards, the period range would also have tightened. Future research will explore this aspect further.

The third phase of the formulation involved controlling collapse safety. Several assumptions were needed to utilise the SPO2IDA tool (Vamvatsikos and Cornell 2005) regarding the structural system’s expected SPO behaviour. Following the suggestions outlined in Sect. 3.2.3, the values shown in Fig. 11 were adopted. For the sake of comparison with other presented formulations, only β_{RTR} was considered for what concerns uncertainty. The collapse fragility was calculated based on the 50th percentile as the median and the β_{RTR} based on the percentile values shown. Following Eqs. (16)–(20), the Sa_y was optimised to 0.37 g for the case 4 structure, meaning that λ_c equated $\lambda_{c,target}$.

Following Sect. 3.2.4, with the identified Sa_y , assuming an initial overstrength q_s of 1.0, the design base shear was calculated with Eq. (21). The design lateral forces were obtained using Eq. (23) and the ELF method was performed to compute member design forces. Strength hierarchy, local ductility requirements and P-Delta effects were all accounted for following the EC8 (CEN 2004b) recommendations and structural elements were verified via their moment–curvature relationships using Response-2000 (Bentz 2015) and EC2 (European Committee for Standardization (CEN) 2004a) material properties. It is important to note, that in the event of the actual SPO of the structure changing, the SPO curve in Fig. 11 and q_s need to be verified and potentially updated to reflect the actual structural properties. The final design solutions in terms of the T_1 and Sa_d are shown in Table 6.

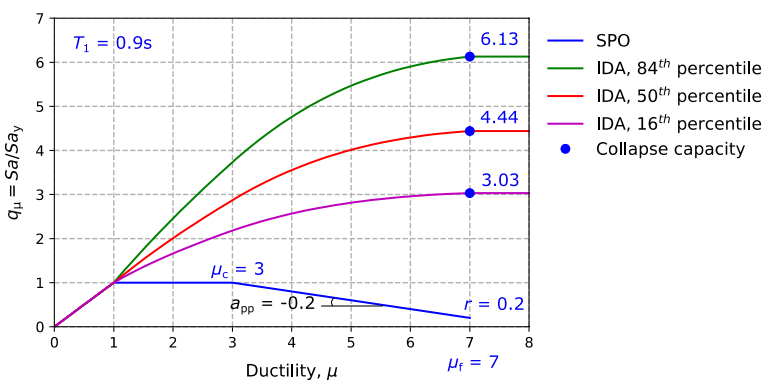


Fig. 11 SPO and IDA curves attained via the SPO2IDA tool

Table 6 Summary of the design solutions from the proposed IPBSD

Case	$\lambda_{c,target}$	T_1 (s)	Sa_d (g)
1	5.0×10^{-4}	0.8	0.24
2	1.0×10^{-4}	0.7	0.54
3	5.0×10^{-4}	1.0	0.18
4	1.0×10^{-4}	0.9	0.47
5	5.0×10^{-4}	1.3	0.09
6	1.0×10^{-4}	0.8	0.48
7	5.0×10^{-4}	1.3	0.09
8	1.0×10^{-4}	1.0	0.38
9	5.0×10^{-4}	1.6	0.08
10	1.0×10^{-4}	1.4	0.27

Table 7 Variation of $Sa^{c,X}$ with X and $\lambda_{c,target}$ for a $\beta=0.5$ (with the exception of ASCE 7-16, where $\beta=0.6$), $T_1=0.7$ s and $q=3.9$ (with the exception of ASCE 7-16, where $q=4.5$)

Assumption	$\lambda_{c,target}$	X	Source for X	$Sa^{c,X}$ (g)	Sa_d (g)
Case study equivalent	5.0×10^{-4}	1.0×10^{-5}	–	0.18	0.05
	1.0×10^{-4}	1.0×10^{-5}		0.40	0.10
	5.0×10^{-4}	1.0×10^{-4}		0.23	0.06
	1.0×10^{-4}	1.0×10^{-4}		0.52	0.13
	5.0×10^{-4}	1.0×10^{-1}		0.78	0.20
	1.0×10^{-4}	1.0×10^{-1}		1.76	0.45
ASCE 7-16	2.0×10^{-4}	1.0×10^{-1}	Luco et al. (2007)	1.21	0.27
EC0	1.0×10^{-5}	1.0×10^{-5}	Douglas et al. (2013)	1.28	0.33

6.5 RTS approach

The approach proposed by Luco et al. (2007) for risk-targeted spectra relies heavily on the underlying assumptions regarding the choice of the probability of collapse, X , and $\lambda_{c,target}$ with respect to the reference hazard, H_{ref} (i.e. 1/475 years), as discussed by Gkimprixis et al. (2019). Here, the risk-targeted spectral acceleration, $Sa^{c,X}$, was computed and then reduced by the code behaviour factor, q , corresponding to EC8’s DCM, to obtain Sa_d . Table 7 lists the variation of $Sa^{c,X}$ depending on $\lambda_{c,target}$ and the assumption of X . It shows high sensitivity towards the underlying assumptions and is noted to be insensitive to the choice of other structural parameters (e.g. typology, number of storeys). The values are more in line with those attained in the previous section when $X=1.0 \times 10^{-1}$. This was particularly interesting, since $\lambda_{c,target}$ do not correspond to the recommended values of 2.0×10^{-4} and 1.0×10^{-5} of ASCE 7-16 (2016) and Eurocode 0 (EC0) (European Committee for Standardization (CEN) 2012), respectively. These observations are possibly due to the indirect assumption of H_{ref} where Gkimprixis et al. (2019) showed a high sensitivity of the H_{ref} to $\lambda_{c,target}$ ratio to values of X , dispersion, β_{RTR} , and seismic hazard slope. In other words, depending on which $\lambda_{c,target}$ and H_{ref} the designer is using, the recommended values should have also been made using those same values. Following the suggestions of Douglas et al. (2013), $Sa^{c,X}$ were recomputed and a large difference was noted. The EC0 assumption of λ_c is stricter, hence the much

higher Sa_d . The value from ASCE 7-16, where $q = 3/2R = 4.5$, assuming R equal to 3 for ordinary RC moment frames (ASCE 7-16 2016), is of a similar magnitude. If one were to follow the results of RTS, the RC frame designed for 0.07 g would most likely not meet the collapse safety condition, as the results presented in Sect. 7.1 will later imply. The designs consistent with EC0 and ASCE 7-16 are more reasonable, and much higher than the values of EC8 obtained in Tables 5 and 6, due to the stricter $\lambda_{c,target}$. Of importance is the fact that the $\lambda_{c,target}$ corresponding to ASCE 7-16 is more lenient as opposed to EC0, and is of similar level with respect to previously attained values through risk-targeted approaches. However, the lack of design flexibility and disregard towards other characteristics of the building (i.e. number of storeys, typology etc.) should not be neglected.

6.6 Summary

For a brief comparison of the case study designs in the previous sections, the Sa_d values obtained from each method are presented in Table 8. A disparity is apparent among the risk-targeted and non-targeted approaches. These latter cases tend to be an order of magnitude higher, albeit with shorter periods. A notable exception is the RTS approach (X of 1.0×10^{-5} , β of 0.5, q of 3.9 and T_1 taken as the FBD cases), which is lower than the others and is most likely due to the inconsistencies in assumptions made while applying the method here, as mentioned above. It is noted that the DDBD and RTS design solutions are not examined further in the interest of space limitations. It is envisaged that due to their relative similarity in terms of Sa_d and T_1 with the FBD solutions, that the range of collapse risk values found for these will be generally applicable to each of these methods. Further analysis showed that this was indeed the case. Of note are the low values of Sa_d associated with methods like EC8 and RTS for some cases when compared to other methods. This is a reflection of the corresponding high T_1 values of these cases, where the design lateral demands reduced due to the higher flexibility of these structures. It is important to note that for EC8, for example, the design T_1 was a parameter that was initially estimated and refined without any constraints. This meant that structures could end up very flexible but still respect the seismic design requirements set out, as was the case here. However, it is important to note that design methods such as EC8 would also have other requirements such as wind and snow loads, amongst others, to take into consideration and would likely affect the final stiffness of the building. These were not considered here in order to isolate and examine the specific outcomes of the seismic design approach without any other non-seismic constraints masking the results obtained.

7 Analysis results

Each case study design was modelled as described in Sect. 5.2 and IDA was performed to characterise the structural behaviour up to lateral collapse using the ground motions described in Sect. 5.3. With this, the actual λ_c with respect to the $\lambda_{c,target}$ is assessed to evaluate each method in delivering sufficiently safe and uniform risk design solutions. The λ_c values were computed with Eq. (20) using the hazard described in Sect. 5.3 and are shown in Table 9, illustrated in Fig. 12 and discussed below.

Table 8 Comparison of the design spectral acceleration, Sa_d , obtained for different frameworks

Cases	$\lambda_{c,target}$	EC8		DDBD		RTS		RTSA-D, TA		RTSA-I, TA		IPBSD		
		T_1 (s)	Sa_d (g)	G, Sa_d (g)	T_1 (s)	Sa_d (g)	T_1 (s)	Sa_d (g)	T_1 (s)	Sa_d (g)	T_1 (s)	Sa_d (g)	T_1 (s)	Sa_d (g)
1	5.0×10^{-4}	1.1	0.10	0.16	0.7	0.12	1.1	0.03	0.7	0.36	0.7	0.43	0.8	0.24
2	1.0×10^{-4}	1.1	0.11	0.27	0.7	0.17	1.1	0.06	0.5	0.91	0.4	1.13	0.7	0.54
3	5.0×10^{-4}	2.3	0.04	0.13	0.7	0.05	2.3	0.01	0.7	0.39	0.9	0.38	1.0	0.18
4	1.0×10^{-4}	2.3	0.05	0.15	0.7	0.08	2.3	0.02	0.7	0.72	0.5	0.855	0.9	0.47
5	5.0×10^{-4}	1.8	0.06	0.14	1.0	0.06	1.8	0.02	1.0	0.30	1.1	0.24	1.3	0.09
6	1.0×10^{-4}	1.8	0.07	0.16	1.0	0.09	1.8	0.03	1.0	0.52	0.7	0.91	0.8	0.48
7	5.0×10^{-4}	2.3	0.05	0.08	0.7	0.06	2.3	0.01	0.7	0.48	1.1	0.25	1.3	0.09
8	1.0×10^{-4}	2.3	0.05	0.09	0.7	0.07	2.3	0.02	0.7	0.80	0.6	1.20	1.0	0.38
9	5.0×10^{-4}	3.0	0.03	0.06	0.9	0.06	3.0	0.01	1.0	0.34	1.1	0.27	1.6	0.08
10	1.0×10^{-4}	3.0	0.04	0.07	0.9	0.07	3.0	0.01	0.8	0.81	0.8	0.78	1.4	0.27

Table 9 Summary of the λ_c for each case study structure and design approach considered

Cases	$\lambda_{c,target} \times 10^{-4}$	IPBSD, $\times 10^{-4}$	$EC8, \times 10^{-4}$			$RTSA, \times 10^{-4}$			
			Impor- tance class	No G	G	D		I	
						TA	TB	TA	A
1	5.0	4.2	II	8.3	6.1	0.8	13.8	1.3	1.3
2	1.0	0.9	III	25.5	5.3	0.1	4.2	0.1	0.1
3	5.0	4.0	II	1.5	5.4	0.9	3.2	1.7	1.9
4	1.0	0.8	III	3.1	4.5	0.3	2.1	0.1	0.2
5	5.0	4.2	II	5.3	4.4	1.8	8.2	2.1	2.5
6	1.0	0.8	III	5.9	3.9	0.5	3.9	0.2	0.3
7	5.0	3.4	II	2.5	4.5	2.7	8.7	2.0	1.4
8	1.0	1.0	III	1.5	3.7	0.1	2.6	0.2	0.1
9	5.0	3.4	II	1.2	1.9	1.9	5.0	2.6	1.0
10	1.0	0.7	III	0.8	1.5	0.8	5.1	0.3	0.3

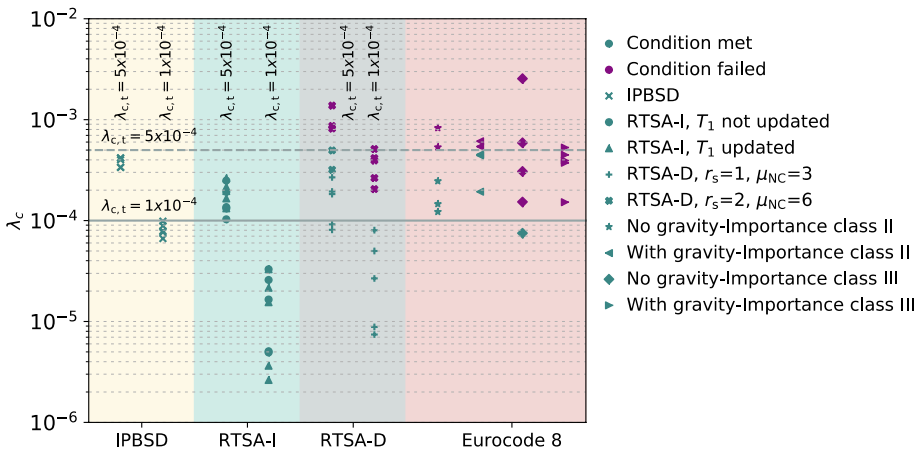


Fig. 12 Illustration of the λ_c values for each case study structure and design approach considered, where for each group of designs the target value is denoted by the vertical text at the top of the plot

7.1 FBD according to EC8

All EC8 design solutions showed similar performance in terms of collapse safety with some scatter among the values. Values ranged from 0.8 to 25.5×10^{-4} for the cases without gravity load considerations and from 1.5 to 6.5×10^{-4} for the cases with gravity load considerations. These are comparable with other values observed in past studies for similar typologies in Italy; Iervolino et al. (2018) examined several structural typologies designed using the Italian building code (NTC) (NTC 2018) and computed λ_c values for RC frames in the order of 10^{-3} and 10^{-4} , which were also similar to the findings for perimeter RC frames of Haselton and Deierlein (2007, chapter 6). As shown in Fig. 12, less than 50% of the case study frames met the $\lambda_{c,target}$. This was not a surprising result given that λ_c did not directly feature as a design input in the FBD method.

The importance class was anticipated to provide an additional degree of collapse safety, although no notable reduction in λ_c was observed. As shown in Table 9, λ_c for some of the importance class II cases were lower compared to importance class III cases, which was an unexpected result. This was due to the difference in provided ductility capacity. For a fixed T_1 and higher design spectral acceleration in importance class III cases (Table 3), the member reinforcement ratios tended to be higher meaning the member curvature ductility capacities decreased. This translated to an overall lower system ductility, meaning the λ_c of structures with higher importance class tending to be higher. This observation highlights the careful balance between strength, stiffness and ductility in seismic design and illustrates that increasing the strength and stiffness of structural members in the name of improved collapse safety is not always an effective solution.

To better visualise this observation, a general trend may be observed via Fig. 13. Using Response-2000 (Bentz 2015), moment–curvature relationships were attained and the variation of curvature ductility capacity, μ_ϕ , is plotted with respect to cross-section effective area, A_{eff} , and tensile reinforcement ratio, ρ . For a fixed value of ρ , taken as a rough proxy for the lateral resistance of a structure, an increase in A_{eff} is needed to increase μ_ϕ . Additionally, μ_ϕ can be increased by reducing ρ for a fixed value of A_{eff} . Therefore, by reducing A_{eff} of importance class II frames, one would essentially increase ρ resulting in decreased μ_ϕ . With the same logic, the resulting λ_c of those frames would be expected to increase.

By adding gravity loads, the collapse safety of the frames did not improve significantly. For example, the best performing structure showed a $\lambda_c = 7.5 \times 10^{-5}$, which was meeting the $\lambda_{c,\text{target}}$ of 5.0×10^{-5} , with the addition of gravity loads during design failing to meet the target. The reasons for such a scenario are likely related to similar conclusions made for the consideration of higher importance class, since by increasing the resistance, the performance of the frame is not necessarily improved. Through the inclusion of gravity loads during design, not only did the demands on the elements increase but also the overstrength factors by an average of 35%, which is in a way akin to having a higher importance class. Since there is no direct control to meet $\lambda_{c,\text{target}}$ values, one may argue that the FBD method currently prescribed by EC8 is not suitable for uniform risk solutions. It must be stated that the aim here was not to diminish current code provisions, but rather highlight the absence of risk-targeted procedures which should be the focus of future development.

7.2 RTSA method

For the RTSA method, it is noted from Fig. 12 that both formulations tended to provide the desired collapse safety by meeting $\lambda_{c,\text{target}}$ due to the inherent risk-targeted of the formulation. A fair degree of scatter among results and conservatism is noted for some cases. Structures designed following both formulations generally performed well with the exception of the RTSA-D TB cases. These discrepancies were mainly as a result of the assumptions made for the overstrength and ductility capacity at the no-collapse limit state. Of importance are also the assumptions regarding the conversion factors needed to move from the collapse to no-collapse limit state (i.e. r_s , μ_{NC} and γ_{ls}), where if incorrectly assumed, disagreement may be anticipated. The design cases presented here were iterated for T_1 only, which for RTSA-I cases seemed to have little impact. Any additional iteration required via SPO analysis or NLRHA to further refine the assumptions of r_s , μ_{NC} and γ_{ls} were not performed, which is important to bear in mind. To this end, the assumed values of r_s , μ_{NC} , γ_{ls} and β_{RTR} were checked against the true behaviour of the frames and how much discrepancy existed.

Figure 14a compares the observed γ_{ls} values against those proposed by Dolšek et al. (2017), where large differences can be observed in some cases but without any consistent trend. This parameter has a notable impact when estimating the actual collapse capacity. Likewise, Fig. 14b compares the dispersions from the model proposed by Dolšek et al. (2017) to those observed here. The observed β_{RTR} values follow the proposed model trend to a certain extent but the values tend to stabilise later at around $T_1=0.9$ s, as opposed to 0.6 s as suggested. Relatively few cases had $\beta_{RTR}>0.4$, while the majority had slightly lower values. This, in addition to an underestimated γ_{ls} , contributed to a decrease in the observed λ_c of the frames and helps explain the conservative nature of some of the results shown in Fig. 12. In any case, the assumption of $\beta_{RTR}=0.4$ is still a reasonable first estimate for most design cases but some instances where validation and possible design iteration would be needed were noted. Additionally, the assumption of equal β_{RTR} for both the CLS and NC limit state (denoted as NCLS in Fig. 14), which is an inherent assumption of the RTSA methods, does not always appear to be a valid one. They are generally close but a notable difference could have a significant impact in the definition of collapse capacity fragility (Fig. 14b). This observation just concerns the record-to-record variability in response but is noted to be only one of many pertinent sources of uncertainty in seismic response.

To evaluate the assumptions of r_s and μ_{NC} used in the RTSA methods, Fig. 15 plots the values obtained from an SPO analysis of the finalised designs. Observing Fig. 15a, the actual values were relatively independent of the initial design assumption and were observed to be between the trialed values of $r_s=1$ and 2, which is in line with the findings of Haselton and Deierlein (2007, chapter 6), where the overstrength of the perimeter RC frames, defined as the ratio of ultimate base shear to design base shear, was

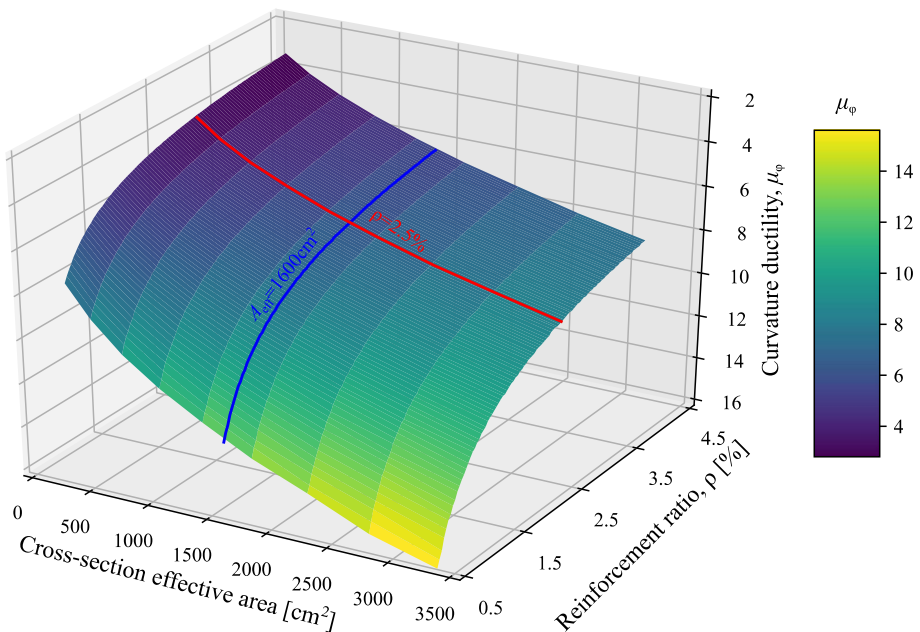


Fig. 13 Interaction of curvature ductility capacity, μ_ϕ , with respect to cross-section effective area, A_{eff} , and tensile reinforcement ratio, ρ , as per EC2 for square columns with symmetric B500C reinforcement, C25/30 concrete, with μ_ϕ computed as the ratio of curvatures at peak and yield moment

between 1.5 and 1.8, meaning that the overstrength defined herein as the base shear at yield to design base shear should be generally lower. In contrast, the overstrength of space frames had a trend with the number of storeys. It is important to note, that no consideration was given to the hardening slope of the backbone behaviour (i.e. elastic-perfectly plastic idealisation was assumed) of the structures of RTSA, which is important for identifying the collapse safety of the structure (Vamvatsikos et al. 2009). Based on the evidence here displayed, the values of overstrength are hard to identify as they depend on parameters like perimeter/space frame, number of storeys and the hardening behaviour of the structure. The under- and overestimation of r_s was seen to have contributed largely to the conservativeness observed for some of the RTSA cases in Fig. 12. Figure 15b, on the other hand, does not show any trend or consistency in the μ_{NC} values with most conservatively exceeding the design assumption with the exception of D-TB cases. Unlike the parameters evaluated in Fig. 14, the assumptions of r_s and μ_{NC} may be evaluated and checked using the results of SPO analysis, possibly requiring multiple design iterations.

7.3 Proposed IPBSD formulation

For what concerns the proposed IPBSD formulation, consistent results were obtained in each case, as shown in Fig. 12. The actual λ_c computed from IDA met the $\lambda_{c,target}$ set within a relatively narrow tolerance and without any case of excessive overdesign. This result demonstrated the proposed IPBSD's efficiency in obtaining risk-targeted design solutions. Furthermore, the median values of collapse capacity observed in IDA matched those identified during design very well and were seen to be independent of any structural characteristics. Figure 16 gives the medians, η , and the β_{RTR} of the collapse capacities of the design cases. The β_{RTR} values established from IDA were first compared to the ones assumed via SPO2IDA during the design process. Similar to RTSA in Fig. 14b, some conservatism of design assumptions of β_{RTR} may be observed in Fig. 16a, but still quite close to actual values and within acceptable bounds; possible iterations could be performed for more refined accuracy. The η used in design were slightly conservative compared to the actual model values (Fig. 16b), possibly due to

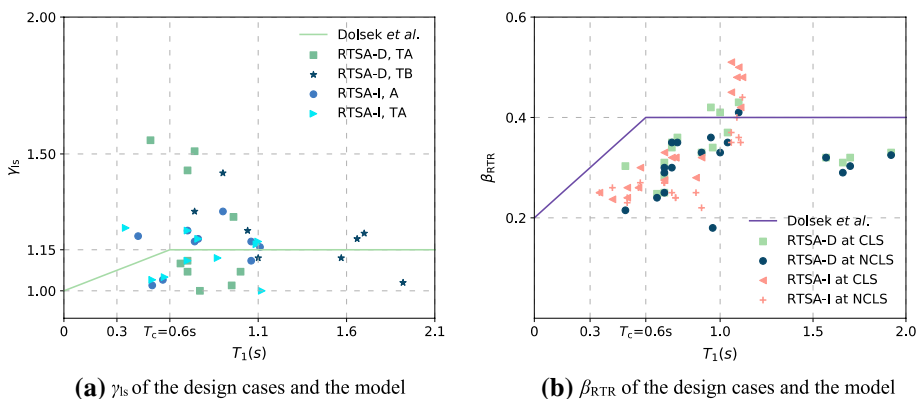


Fig. 14 Comparison of the Dolšek et al. model values for **a** γ_{Is} and **b** β_{RTR} as a function of T_1 provided by Dolšek et al. (2017) with the actual values computed from IDA upon designing and detailing

slight overstrength or ductility in the structures, or due to the approximate nature of the SPO2IDA tool, but were nonetheless found to be sufficiently accurate to result in suitable and efficient design solutions.

The assumed and calculated overstrength values of q_s (Fig. 3) from SPO analysis are presented in Fig. 17. As one may notice, the actual values of q_s are not that different from the initial design assumption. For case study frames 5, 7, 9, the design q_s was updated as an additional iteration was required to increase the accuracy of the method. After the initial design of those frames, notable overstrength were inherent due to strong-column weak-beam requirement and local ductility requirement of EC8. To satisfy the demands of ELF, the required longitudinal reinforcement ratio was below the limit value, hence, it was increased to match the demands of the code, thus resulting in relatively high overstrength of the overall structure. For the other frames, where overstrength was relatively negligible, no iteration was performed and was found to have negligible effects on the results. However, as already pointed out in Sect. 7.2, iterations might be necessary for the accurate estimation of q_s , specifically when gravity loads are involved in design, and a certain level of overstrength is expected when any seismic code provisions are utilised.

7.4 Refined estimate of collapse risk

One of the assumptions of the proposed IPBSD method (and all others evaluated here) was that using $Sa(T_1)$ as an IM and IDA with the ground motions identified in Sect. 5.3 was a suitable strategy for estimating collapse risk. Research in recent years has indicated that this may not be the most robust approach and other IM definitions may be more suitable (e.g. the spectral acceleration at some multiple of T_1 or averaged range around it) and other ground motion selection techniques (Baker 2011) may be more suitable. Eads et al. (2015) have shown that spectral acceleration averaged over a period range around T_1 , $AvgSa$, is a more efficient IM in collapse risk estimation. Ideally, this IM would be used here but given the simplicity and physical meaning of $Sa(T_1)$ in relation to the design base shear, this simpler option was preferred. Nevertheless, the question remains as to whether using $Sa(T_1)$ as the IM in an IDA with a single set of ground motion records still meets the collapse risk when characterised using more refined, but cumbersome, methods of collapse risk quantification? To shed some light on this, the λ_c of the IPBSD case frames was recomputed to verify that it was in fact slightly conservative when using $AvgSa$. For what concerns the use

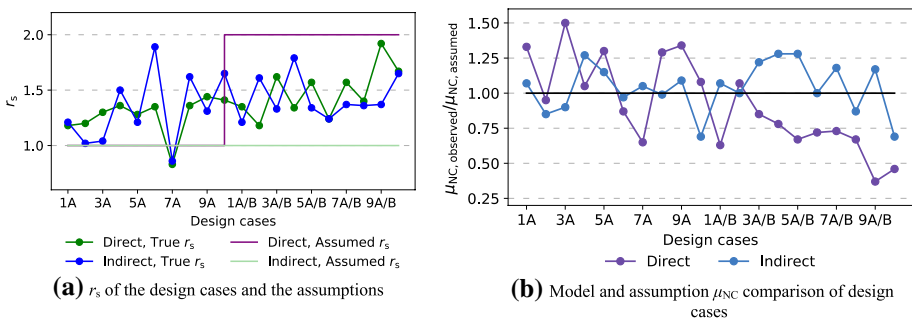


Fig. 15 Comparison of the assumed values for **a** r_s and **b** μ_{NC} ratios, with the actual values computed from SPO upon designing and detailing, where the notation A refers to D-TA and I-A cases, and A/B refers to I-TA/D-TB cases

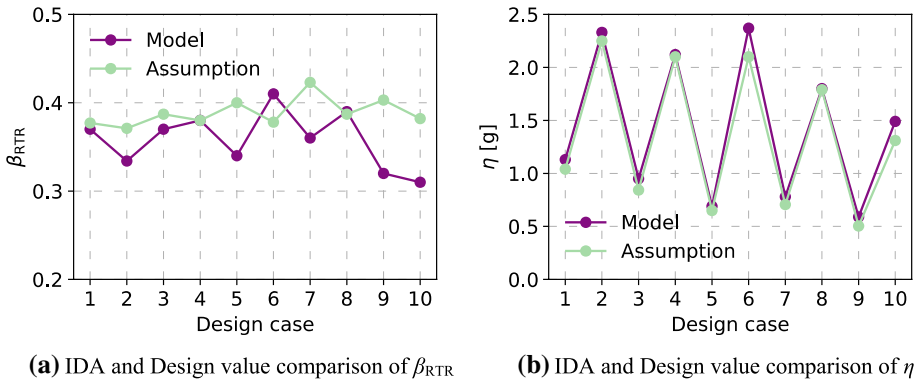


Fig. 16 Comparison of computed and assumed values of **a** β_{RTR} and **b** η at CLS

of a single ground motion record set, Eads et al. (2015) have shown that λ_c estimates were relatively insensitive to different sets when using *AvgSa*. Therefore, if it can be shown that the *AvgSa*-based λ_c values are at least as low as the *Sa*(T_1)-based ones, the design results may be deemed suitable.

To do this, the IDA results previously established were reprocessed for all structures in terms of *AvgSa*, defined within a period range of 0.35 s and 3.55 s with a 0.10 s step for all structures. The distribution of collapse intensities was identified and integrated with the hazard curve associated with *AvgSa* to estimate λ_c . This hazard curve was computed from the same hazard model described in Sect. 5.3. Similar to Eads et al. (2015), collapse dispersions using *AvgSa* were lower and the overall λ_c was on the conservative side. Figure 18 illustrates the results with reference to original values computed and verified in Sect. 7.3. In short, the more refined *AvgSa*-based λ_c values are indeed lower than the *Sa*(T_1)-based ones indicating that the designs established using *Sa*(T_1) are slightly conservative. All methods evaluated here would be expected to show the same trend so it is not envisaged to be a drawback to the specific design method proposed per se, but rather a convenience choice for design. It is worth noting that for their implementation of RTBF (Sect. 4), Vamvatsikos et al. (2020) used *AvgSa* as their IM to address the issue discussed.

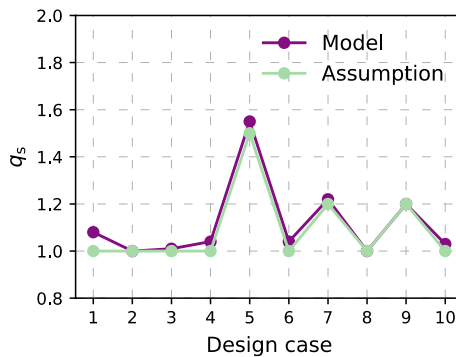


Fig. 17 Comparison of computed and design values of q_s

8 Summary and conclusions

The ability to design structures following a simplified performance-based earthquake engineering (PBEE)-based methodology has been one of the many focusses of the earthquake engineering community. Current design methods, such as those found in many design codes, deal with design without adequately accounting for the probabilistic nature of both seismic design input and structural response. In the disciplinary discourse of risk-consistent seismic design approaches, there is a tendency to balance the ease of implementation for practitioners with flexibility and accuracy in identifying risk-consistent design solutions.

This article proposed the integrated performance-based seismic design (IPBSD) framework, allowing the identification of feasible design solutions that limit expected monetary losses and target a given collapse safety. It was described via a step-by-step implementation and tested for several case study RC frame structures. Other existing design code approaches and risk-targeted approaches were described and critically reviewed by comparing some common categories, such as performance objectives, seismic hazard definition, non-linear behaviour treatment, risk-consistency and the flexibility of each method. Many of these methods were also tested for the case study structures examined in order to have a broad and thorough comparison of different approaches. Following a full design of each structure's members, numerical models were developed and non-linear response history analysis was performed through an application of incremental dynamic analysis (IDA). Integrating this IDA response of each structure allowed the actual collapse safety to be quantified and compared with the initial limit targeted in design. The main conclusions of this study are as follows:

- Half of the case study frames following Eurocode 8 met the MAFC condition, which was not surprising given the nature of the non-risk targeted approaches. Even though two importance classes were considered, no significant degree of increased collapse safety was consistently obtained. In fact, some of the importance class II frames performed better than the III ones since, for a fixed fundamental period, the member reinforcement ratios tended to reduce and led to increased member ductility

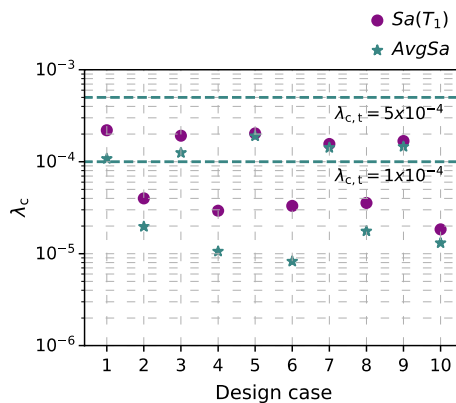


Fig. 18 Illustration of collapse risks using $Sa(T_1)$ or AvgSa as the IM

capacities. This offsets the lower strength to provide a higher collapse capacity via increased ductility. Hence, a careful balance between strength, stiffness and ductility in seismic design is vital and simply increasing the strength and stiffness of structural members in the name of improved collapse safety is not always an effective solution;

- The addition of gravity loads in the design process improved the collapse safety via additional overstrength. However, no consistent trend was observed pointing towards a need for its explicit consideration in design;
- The apparent lack of design flexibility and heavy dependence on the design reference values in current implementations of risk-targeted spectra (RTS) means that underlying assumptions need subsequent modifications to result in widespread adaptation;
- Design and validation of cases following the risk-targeted seismic action (RTSA) method demonstrated the advantages of risk-targeted approaches, as the majority of cases met the MAFC condition. It was found that assumptions regarding design input parameters had a significant impact when targeting a specific collapse safety. Several design cases initially reported collapse risk values much lower than the design target and was found to be as a result of conservative design input parameters, which could be refined through repeated design iterations;
- Many of the assumptions needed for the RTSA method and the proposed IPBSD method require further quantification studies and experimentation for suitable initial design input parameters and targets; specifically, the anticipated collapse capacity uncertainty β_{RTR} , or on how to quantify the expected ductility capacity and the post-capping strength of structural elements. Some research exists on these issues but much more could be done to consolidate the understanding and render them useful in design practice;
- The proposed IPBSD approach demonstrated consistent results in terms of meeting the collapse safety targets for each case study frames. The targets were met with relatively narrow conservatism and without any case of excessive overdesign or requiring multiple design iterations.
- The structures' collapse capacities from IDA (i.e. median and dispersion) were slightly conservative, possibly due to supplementary ductility in the structure or the approximate nature of the SPO2IDA tool (Vamvatsikos and Cornell 2005); however, it was found to be sufficiently accurate to result in suitable and efficient design solutions.

In summary, methods following a risk-targeted approach performed reasonably well, while the cases designed following other traditional approaches, such as Eurocode 8, failed the target collapse safety condition. The beauty of the proposed IPBSD approach is in its flexibility and simplicity, as it combines the advantages of different methods in the literature, including code-based provisions, to give risk-consistent design solutions. It is envisaged that this approach, following further research and refinements, should form a part of the next-generation seismic design approaches aiming to achieve the goals of PBEE.

Author contributions DS: Analysis; Software; Validation; Writing—Initial drafting. GJOR: Conceptualisation; Validation; Supervision; Writing—Initial drafting, editing and reviewing.

Funding The work presented in this paper has been developed within the framework of the project “Dipartimenti di Eccellenza”, funded by the Italian Ministry of Education, University and Research at IUSS Pavia.

Compliance with ethical standards

Conflict of interest The authors declare to have no conflicts of or competing interests.

References

- Ancheta TD, Darragh RB, Stewart JP, Seyhan E, Silva WJ, Chiou BSJ et al (2014) NGA-West2 database. *Earthq Spectra* 30(3):989–1005. <https://doi.org/10.1193/070913EQS197M>
- ASCE 7-16 (2016) Minimum design loads for buildings and other structures. ASCE, Reston, VA, USA
- Aschheim M, Black EF (2000) Yield point spectra for seismic design and rehabilitation. *Earthq Spectra* 16(2):317–335. <https://doi.org/10.1193/1.1586115>
- Baker JW (2011) Conditional mean spectrum: tool for ground-motion selection. *J Struct Eng* 137(3):322–331. [https://doi.org/10.1061/\(ASCE\)ST.1943-541X.0000215](https://doi.org/10.1061/(ASCE)ST.1943-541X.0000215)
- Bentz E (2015) Appendix A: program manuals from sectional analysis of reinforced concrete members by: Graduate Department of Civil Engineering University of Toronto, Canada
- Calvi GM, Sullivan TJ, Welch DP (2014) A seismic performance classification framework to provide increased seismic resilience. *Geotech Geol Earthq Eng*. https://doi.org/10.1007/978-3-319-07118-3_11
- Calvi GM, Rodrigues D, Silva V (2018) Introducing new design spectra derived from Italian recorded ground motions 1972 to 2017. *Earthq Eng Struct Dyn* 47(13):2644–2660. <https://doi.org/10.1002/eqe.3102>
- CEN (2004a) Eurocode 2: Design of concrete structures—part 1-1: general rules and rules for buildings (EN 1992-1-1). CEN, Brussels, Belgium
- CEN (2004b) Eurocode 8: Design of structures for earthquake resistance—part 1: general rules, seismic actions and rules for buildings (EN 1998-1:2004). CEN, Brussels, Belgium
- CEN (2012) Eurocode 0: Eurocode-basis of structural design (EN 1990:2002 + A1). CEN, Brussels, Belgium
- CEN (2018) Eurocode 8: Design of structures for earthquake resistance (draft)—part 1: general rules, seismic actions and rules for buildings (EN 1998-1:2018). CEN, Brussels, Belgium
- CNR (2014) Istruzioni per la Valutazione Affidabilistica della Sicurezza Sismica di Edifici Esistenti. CNR - Commissione di Studio per la Predisposizione e l'Analisi di Norme Tecniche Relative Alle Costruzioni, Rome, Italy (**in Italian**)
- Cook D, Liel AB, Luco N, Almeter E, Haselton C (2019) Implications of seismic design values for economic losses. In: 13th international conference on applications of statistics and probability in civil engineering, ICASP 2019, Seoul, South Korea
- Cornell CA (1996) Calculating building seismic performance reliability: a basis for multi-level design norms. In: 11th World Conference on Earthquake Engineering (11WCEE), Acapulco, Mexico
- Cornell CA, Krawinkler H (2000) Progress and challenges in seismic performance assessment. *PEER Center News* 3(2):1–2
- Cornell CA, Jalayer F, Hamburger RO, Foutch DA (2002) Management agency steel moment frame guidelines. *J Struct Eng* 128:526–533. [https://doi.org/10.1061/\(ASCE\)0733-9445\(2002\)128:4\(526\)](https://doi.org/10.1061/(ASCE)0733-9445(2002)128:4(526))
- Cosenza E, Del Vecchio C, Di Ludovico M, Dolce M, Moroni C, Prota A et al (2018) The Italian guidelines for seismic risk classification of constructions: technical principles and validation, vol 16. Springer, Dordrecht. <https://doi.org/10.1007/s10518-018-0431-8>
- Dolšek M, Lazar Sinković N, Žižmond J (2017) IM-based and EDP-based decision models for the verification of the seismic collapse safety of buildings. *Earthq Eng Struct Dyn* 46(15):2665–2682. <https://doi.org/10.1002/eqe.2923>
- Douglas J, Ulrich T, Negulescu C (2013) Risk-targeted seismic design maps for mainland France. *Nat Hazards* 65(3):1999–2013. <https://doi.org/10.1007/s11069-012-0460-6>
- Duckett W (2004) Risk analysis and the acceptable probability of failure. *Struct Eng* 83:1–5
- Eads L, Miranda E, Lignos DG (2015) Average spectral acceleration as an intensity measure for collapse risk assessment. *Earthq Eng Struct Dyn* 44(12):2057–2073. <https://doi.org/10.1002/eqe.2575>
- Fajfar P (2018) Analysis in seismic provisions for buildings: past, present and future: the fifth Prof. Nicholas Ambraseys lecture, vol 16. Springer, Dordrecht. <https://doi.org/10.1007/s10518-017-0290-8>
- Fajfar P, Dolšek M (2012) A practice-oriented estimation of the failure probability of building structures. *Earthq Eng Struct Dyn* 41:531–547. <https://doi.org/10.1002/eqe>
- FEMA (2000) Prestandard and commentary for the seismic rehabilitation of buildings. FEMA 356, Reston, VA, USA
- FEMA (2009a) Quantification of building seismic performance factors. FEMA P695, Washington, USA

- FEMA (2009b) NEHRP recommended seismic provisions. FEMA P-750, Reston, VA, USA
- FEMA (2012) FEMA P-58-1: seismic performance assessment of buildings: methodology, vol 1. FEMA, Washington, DC
- Gkimprixis A, Tubaldi E, Douglas J (2019) Comparison of methods to develop risk-targeted seismic design maps. *Bull Earthq Eng* 17(7):3727–3752. <https://doi.org/10.1007/s10518-019-00629-w>
- Gokkaya BU, Baker JW, Deierlein GG (2016) Quantifying the impacts of modeling uncertainties on the seismic drift demands and collapse risk of buildings with implications on seismic design checks. *Earthq Eng Struct Dyn* 45(10):1661–1683. <https://doi.org/10.1002/eqe.2740>
- Goulet CA, Haselton CB, Mitrani-reiser J, Beck JL, Deierlein GG, Porter KA et al (2007) Evaluation of the seismic performance of a code-conforming reinforced-concrete frame building—from seismic hazard to collapse safety and economic losses. *Earthq Eng Struct Dyn* 36:1973–1997. <https://doi.org/10.1002/eqe.694>
- Günay S, Mosalam KM (2013) PEER performance-based earthquake engineering methodology, revisited. *J Earthq Eng* 17(6):829–858. <https://doi.org/10.1080/13632469.2013.787377>
- Haselton CB, Deierlein GG (2007) Assessing seismic collapse safety of modern reinforced concrete moment frame buildings. PEER Report 2007/08, Berkeley, USA
- Haselton CB, Liel AB, Taylor-Lange SC, Deierlein GG (2016) Calibration of model to simulate response of reinforced concrete beam-columns to collapse. *ACI Struct J* 113(6):1141–1152. <https://doi.org/10.14359/51689245>
- Ibarra LF, Medina RA, Krawinkler H (2005) Hysteretic models that incorporate strength and stiffness deterioration. *Earthq Eng Struct Dyn* 34(12):1489–1511. <https://doi.org/10.1002/eqe.495>
- Iervolino I, Spillatura A, Bazzurro P (2018) Seismic reliability of code-conforming italian buildings. *J Earthq Eng* 22(sup2):5–27. <https://doi.org/10.1080/13632469.2018.1540372>
- Kennedy RC, Short SA (1994) Basis for seismic provisions of DOE-STD-1020. Livermore, California
- Krawinkler H, Zareian F, Medina RA, Ibarra LF (2006) Decision support for conceptual performance-based design. *Earthq Eng Struct Dyn* 35(1):115–133. <https://doi.org/10.1002/eqe.536>
- Luco N, Ellingwood BR, Hamburger RO, Hooper JD, Kimball JK, Kircher CA (2007) Risk-targeted versus current seismic design maps for the conterminous United States. In: SEAOC 2007 convention proceedings, Squaw Creek, CA
- McKenna F, Scott MH, Fenves GL (2010) Nonlinear finite-element analysis software architecture using object composition. *J Comput Civil Eng* 24(1):95–107. [https://doi.org/10.1061/\(ASCE\)CP.1943-5487.0000002](https://doi.org/10.1061/(ASCE)CP.1943-5487.0000002)
- NTC (2018) Norme Tecniche per le Costruzioni (NTC18). Rome, Italy (in Italian)
- NZS 1170.5:2004 (2004) Structural design actions part 5: earthquake actions. Wellington, New Zealand
- O'Reilly GJ, Calvi GM (2019) Conceptual seismic design in performance-based earthquake engineering. *Earthq Eng Struct Dyn* 48(4):389–411. <https://doi.org/10.1002/eqe.3141>
- O'Reilly GJ, Calvi GM (2020) Quantifying seismic risk in structures via simplified demand-intensity models. *Bull Earthq Eng* 18(5):2003–2022. <https://doi.org/10.1007/s10518-019-00776-0>
- Pagani M, Monelli D, Weatherill G, Danciu L, Crowley H, Henshaw P et al (2014) OpenQuake engine: an open hazard (and risk) software for the global earthquake model. *Seismol Res Lett* 85:692–702. <https://doi.org/10.1785/0220130087>
- Priestley MJN (2003) Myths and fallacies in earthquake engineering, revisited. In: The 9th Mallet Milne lecture. IUSS Press, Pavia, Italy
- Priestley MJN, Calvi GM, Kowalsky MJ (2007) Displacement-based seismic design of structures. IUSS Press, Pavia, Italy
- Ramirez CM, Miranda E (2009) Building specific loss estimation methods & tools for simplified performance-based earthquake engineering. Blume Center Report No. 171, Stanford, USA
- Ramirez CM, Liel AB, Mitrani-Reiser J, Haselton CB, Spear AD, Steiner J et al (2012) Expected earthquake damage and repair costs in reinforced concrete frame buildings. *Earthq Eng Struct Dyn* 41(11):1455–1475. <https://doi.org/10.1002/eqe.2216>
- SEAOC (1995) Vision 2000: performance-based seismic engineering of buildings. Sacramento, California
- Shahnazaryan D, O'Reilly GJ, Monteiro R (2019) Using direct economic losses and collapse risk for seismic design of RC buildings. In: COMPDYN 2019—7th international conference on computational methods in structural dynamics and earthquake engineering, Crete Island, Greece. <https://doi.org/10.7712/120119.7281.19516>
- Silva A (2020) Implications of Earthquake-induced loss control in seismic design provisions. PhD thesis, IUSS Pavia, Italy
- Silva V, Crowley H, Bazzurro P (2016) Exploring risk-targeted hazard maps for Europe. *Earthq Spectra* 32(2):1165–1186. <https://doi.org/10.1193/112514EQS198M>

- Sinković NL, Brozovič M, Dolšek M (2016) Risk-based seismic design for collapse safety. *Earthq Eng Struct Dyn* 45(9):1451–1471. <https://doi.org/10.1002/eqe.2717>
- Sullivan TJ, Calvi GM, Priestley MJN, Kowalsky MJ (2003) The limitations and performances of different displacement based design methods. *J Earthq Eng* 7:201–241. <https://doi.org/10.1080/13632460309350478>
- Vamvatsikos D (2013) Derivation of new SAC/FEMA performance evaluation solutions with second-order hazard approximation. *Earthq Eng Struct Dyn* 42(8):1171–1188. <https://doi.org/10.1002/eqe.2265>
- Vamvatsikos D, Aschheim MA (2016) Performance-based seismic design via yield frequency spectra. *Earthq Eng Struct Dyn* 45(11):1759–1778. <https://doi.org/10.1002/eqe.2727>
- Vamvatsikos D, Cornell CA (2005) Direct estimation of seismic demand and capacity of multidegree-of-freedom systems through incremental dynamic analysis of single degree of freedom approximation. *J Struct Eng* 131(4):589–599. [https://doi.org/10.1061/\(ASCE\)0733-9445\(2005\)131:4\(589\)](https://doi.org/10.1061/(ASCE)0733-9445(2005)131:4(589))
- Vamvatsikos D, Akkar SD, Miranda E (2009) Strength reduction factors for the dynamic instability of oscillators with non-trivial backbones. In: *COMPdyn 2009—ECCOMAS thematic conference on computational methods in structural dynamics and earthquake engineering*, Rhodes Island, Greece
- Vamvatsikos D, Kazantzi AK, Aschheim MA (2016) Performance-based seismic design: avant-garde and code-compatible approaches. *ASCE-ASME J Risk Uncertain Eng Syst Part A Civ Eng*. <https://doi.org/10.1061/AJRUA6.0000853>
- Vamvatsikos D, Bakalis K, Kohrangi M, Pyrza S, Castiglioni CA, Kanyilmaz A et al (2020) A risk-consistent approach to determine EN1998 behaviour factors for lateral load resisting systems. *Soil Dyn Earthq Eng*. <https://doi.org/10.1016/j.soildyn.2019.106008>
- Woessner J, Wiemer S (2005) Assessing the quality of earthquake catalogues: estimating the magnitude of completeness and its uncertainty. *Bull Seismol Soc Am* 95(2):684–698. <https://doi.org/10.1785/0120040007>
- Zareian F, Krawinkler H (2012) Conceptual performance-based seismic design using building-level and story-level decision support system. *Earthq Eng Struct Dyn* 41(11):1439–1453. <https://doi.org/10.1002/eqe.2218>
- Žižmond J, Dolšek M (2019) Formulation of risk-targeted seismic action for the force-based seismic design of structures. *Earthq Eng Struct Dyn*. <https://doi.org/10.1002/eqe.3206>

Publisher's Note Springer Nature remains neutral with regard to jurisdictional claims in published maps and institutional affiliations.